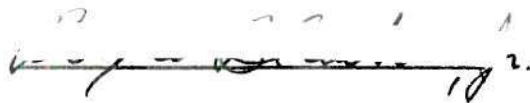


In presenting the dissertation as a partial fulfillment of the requirements for an advanced degree from the Georgia Institute of Technology, I agree that the Library of the Institution shall make it available for inspection and circulation in accordance with its regulations governing materials of this type. I agree that permission to copy from, or to publish from, this dissertation may be granted by the professor under whose direction it was written, or, in his absence, by the dean of the Graduate Division when such copying or publication is solely for scholarly purposes and does not involve potential financial gain. It is understood that any copying from, or publication of, this dissertation which involves potential financial gain will not be allowed without written permission.

 2.

FLOW DISTRIBUTIONS OF A PERFECT GAS  
FROM MANIFOLDS WITH ISOTHERMALLY HEATED WALLS

A THESIS

Presented to  
the Faculty of the Graduate Division  
by  
Roy Warner Blanton, Jr.

In Partial Fulfillment  
of the Requirements for the Degree  
Doctor of Philosophy in the School  
of Mechanical Engineering

Georgia Institute of Technology

April, 1963

FLOW DISTRIBUTIONS OF A PERFECT GAS  
FROM MANIFOLDS WITH ISOTHERMALLY HEATED WALLS

Approved

*[Handwritten signature]*

Dr. Thomas W. Jackson, Chairman

*[Handwritten signature]*

Dr. Charles W. Gorton

*[Handwritten signature]*

Dr. William B. Harrison

Date Approved by Chairman 6 May 1963

68  
12 R 11

To My Wife

ESTELLE MALOY BLANTON

Whose Love, Patience, and Encouragement Have  
Been the Predominant Factors in Making this  
Work Possible.

## ACKNOWLEDGMENTS

The author wishes to make the following acknowledgments: To Dr. Thomas W. Jackson of the Engineering Experiment Station for his interest, assistance, and guidance throughout the course of this work; to Dr. Charles W. Gorton of the School of Mechanical Engineering for his suggestions and help with the manuscript; and to Dr. William B. Harrison of the School of Nuclear Engineering for reviewing the manuscript.

## TABLE OF CONTENTS

	Page
DEDICATION . . . . .	ii
ACKNOWLEDGEMENTS . . . . .	iii
Chapter	
I. INTRODUCTION . . . . .	1
II. DEVELOPMENT OF THE MATHEMATICAL EQUATIONS . . . . .	4
III. SOLUTION OF THE MATHEMATICAL EQUATIONS . . . . .	15
IV. EQUIPMENT . . . . .	20
V. TEST PROCEDURE . . . . .	24
VI. ANALYSIS OF RESULTS . . . . .	27
VII. CONCLUSIONS AND RECOMMENDATIONS . . . . .	31
APPENDIX . . . . .	33
I. THE DIFFERENTIAL EQUATIONS . . . . .	34
II. THE CALIBRATION AND CORRELATION OF THE PITOT TUBES . . . . .	41
III. DATA . . . . .	45
IV. SAMPLE PROBLEM . . . . .	94
NOMENCLATURE . . . . .	97
BIBLIOGRAPHY . . . . .	100
VITA . . . . .	102

## CHAPTER I

## INTRODUCTION

The flow distributions from a manifold with heat transfer find application in heat exchangers and manifold systems for internal combustion engines.

The manifold problem has been solved extensively, both analytically and experimentally, for an incompressible, isothermal fluid. Keller (1)\* studied the general problem of a manifold discharging fluid through several openings along the manifold length and supplying fluid to a set of parallel pipes or ducts at right angles to the axis of the manifold. Both mathematical and experimental studies found that, for perforated pipes, the discharge profile was essentially determined by the relative values of pressure regain arising from deceleration and by the pressure loss caused by friction.

The curves given by Keller show that, as the diameter of the pipe increases relative to its length, it is possible to reach a stage at which the quantity leaving the holes at the downstream end of the pipe is considerably greater than that from the holes at the upstream end.

Dow (2) considered the question in connection with the design of pipe burners. He realized that the change of flow pattern occurring in

---

\*Numbers in parentheses refer to the Bibliography.

the passing from turbulent to streamline motion in the pipe may completely alter the distribution of velocity from the jets. He solved mathematically the special case of a constant rate of discharge along the length of the manifold. Dow adopted a pipe of constant diameter and with uniform holes at constant pitch. In order to achieve the same level of flame along the length of the gas burner, he inserted a tapered plug, thus varying the effective passage available to the gas as it passed from one end of the pipe to the other.

Acrivos, Babcock, and Pigford (3) investigated the variation of static pressure along the main channel of a manifold and the distribution of the fluid flowing through the ports for both a "blowing" and a "sucking" manifold. The curves given by them represent the mathematical solution for a manifold with zero distance between ports and show that for certain configurations the distribution of fluid through the ports may be made very nearly uniform. These curves also show the effect of a finite distance between ports on the flow distribution.

Allen and Albinson (4) have described a similar but simpler mathematical approach to that of Keller (1), in which finite changes in pressure and velocity between the individual discharge ports of a manifold are considered. They have given a formula for the variation required in the port areas along the pipe if the discharge quantity is to be uniform.

Safar (5) studied experimentally the effect on the flow distribution of heating the ports of a manifold. The curves which he presented show that the mass flow rate is reduced by up to 11% when the port is heated. Safar's data are presented for only one heated port at a time,



This then leads to the problem at hand, which is the determination of the flow distribution when the whole manifold is heated.

The author proposes to study mathematically the flow distribution of a perfect gas from manifolds with isothermally heated walls. The study will be based upon a one-dimensional analysis of the flow, with the solutions to the equations being obtained with the aid of an electronic computer.

Experimentally, the flow distribution from the heated manifold will be determined by measuring the mean velocity across the port for various values of total mass flow rate, ratios of port area to cross-sectional area, and ratios of inlet temperature to wall temperature.

## CHAPTER II

## DEVELOPMENT OF THE MATHEMATICAL EQUATIONS

The non-dimensional equations governing the flow may be written when the following assumptions are made:

1. The fluid is a perfect gas.
2. The effect of compressibility on the flow through the port may be neglected.
3. The effect of the variation in pressure upon the density is small compared with the effect of the variation in temperature.
4. The wall temperature is a constant.
5. The friction factor is a constant.

Equations for the Discrete Blowing Manifolds.---Beginning with the closed tube section (see Figure 1) of the manifold, an equation (see Shapiro (6)) for the variation in pressure as a result of changes in stagnation temperature and friction may be written,

$$\frac{dp}{p} = - \frac{kM^2(1 + \frac{k-1}{2} M^2)}{1-M^2} \frac{dT'}{T'} - \frac{kM^2 [1 + (k-1)M^2]}{2(1-M^2)} \frac{4f dx}{D}.$$

When low speed flow is considered,  $M^2 \ll 1$  and  $M^4 \ll M^2$  (see Nomenclature for a definition of the symbols),

$$\frac{kM^2(1 + \frac{k-1}{2} M^2)}{1-M^2} \approx kM^2$$

and

$$\frac{kM^2 [1+(k-1)M^2]}{2(1-M^2)} \approx \frac{kM^2}{2} .$$

The relation is then

$$\frac{dp}{p} = \frac{-kM^2 dT'}{T'} - kM^2 \frac{2f dx}{D} .$$

A further simplification results when Reynolds analogy between friction and heat transfer is assumed valid. Using Reynolds analogy in the form

$$\frac{dT'}{T_w - T'} = \frac{2f dx}{D}$$

along with

$$kM^2 = \frac{\rho u^2}{p} ,$$

the desired relationship becomes

$$\frac{dp}{p} = \frac{-\rho u^2}{p} \left[ 1 + \frac{T_w - T'}{T'} \right] \frac{2f dx}{D}$$

or

$$dp = -\rho u^2 \left[ \frac{T_w}{T'} \right] \frac{2f dx}{D} .$$

For low speed flow  $T' \approx T$ , also let  $T_i = T$

where  $x = i$ . Then

$$dp = -\rho u^2 \left[ \frac{T_w}{T} \right] \frac{2f}{D} dx \quad .$$

Now using the following:

$$\frac{w}{A} = \rho u = \text{constant}, \quad f \text{ and } T_w \text{ are constants},$$

and integrating

$$p_i' - p_i^o = -\frac{2f}{D} \rho_i u_i^o \int_{x=(i-1)\Delta x}^{x=i\Delta x} u \frac{T_w}{T} dx \quad .$$

The integration of  $u \frac{T_w}{T}$  can be obtained in a closed form if  $u$  is replaced by an average value of  $u$ . Let the average value of  $u$  be given

by  $\frac{u_i^o + u_i'}{2}$ , then

$$p_i' - p_i^o = -\frac{2f}{D} \rho_i u_i^o \left( \frac{u_i^o + u_i'}{2} \right) \int_{x_1}^{x_2} \frac{T_w}{T} dx \quad .$$

From Shapiro (see Ref. 6, P. 243)

$$T = T_w - (T_w - T_o) e^{-\frac{2fx}{D}}$$

then

$$\int_{x_1}^{x_2} \frac{T_w}{T} dx = x + \frac{D}{2f} \ln \left( 1 - \frac{T_w - T_o}{T_w} e^{-\frac{2fx}{D}} \right) \Bigg|_{x_1}^{x_2} .$$

Now using the dimensionless quantities

$$\Theta_i = \frac{T_i}{T_w}, \quad \phi_i = \frac{\rho_i}{\rho_o}, \quad P_i^o = \frac{(p_i^o - p_s)}{2\beta \rho_o u_o^2},$$

$$U_i = \frac{u_i^o}{u_o}, \quad F_i = \frac{f_i}{2^{5/2} \beta^{3/2} \alpha_K}, \quad \text{and } y = \frac{4\alpha_K}{D} \sqrt{2\beta} \Delta x,$$

the relationship for the variation in pressure as a result of changes in stagnation temperature and friction is obtained in the non-dimensional form

$$P_i' - P_i^o = -\Theta_i U_i^o \frac{(U_i^o + U_i')}{2} \left[ F_i \Delta y + G_i \right] \quad (1-A)$$

where

$$G_i = \frac{1}{2\beta} \ln \frac{\Theta_{i+1}}{\Theta_i}. \quad (2-A)$$

Next, by writing a material balance and using the orifice equation about the port (see Figure 2), the following is obtained:

$$\Delta w = A \left[ (\rho u)_{i+1}^o - (\rho u)_i^i \right]$$

also

$$\Delta w = -\alpha \pi D \Delta x K \sqrt{2 \rho (p - p_s)}$$

where

$K$  = coefficient of discharge

$\alpha$  = fraction of internal surface area of tube that is occupied by discharge ports, assumed uniformly spaced along the tube

$\alpha \pi D \Delta x$  = discharge area of the port.

The subscript  $s$  refers to the surroundings. Now equating the two, the relationship becomes,

$$(\rho u)_{i+1}^o - (\rho u)_i^i = - \frac{\alpha \pi D \Delta x K}{A} \sqrt{2 \rho (p - p_s)} .$$

If an average pressure is used for  $p$ ,  $p = \frac{p_i^i + p_{i+1}^o}{2}$ ,

and the effect of the variation in pressure upon the density is assumed small compared with the effect of the variation in temperature,

$$\rho_{i+1}^o = \rho_i = \rho_{i+1}^i ,$$

then

$$u_{i+1}^o - u_i^i = - \frac{4 \alpha K \Delta x}{D} \sqrt{\frac{2}{\rho_{i+1}} \left( \frac{p_i^i + p_{i+1}^o}{2} - p_s \right)} .$$

The relation upon non-dimensionalization becomes

$$U_{i+1}^o - U_i^i = -\Delta y \sqrt{\frac{P_{i+1}^o + P_i^i}{\theta_{i+1}}} . \quad (3-A)$$

Now, another relation is obtained from a momentum balance as indicated in Figure 2,

$$P_{i+1}^o - P_i^i = \theta \rho_{i+1} [U_i^{i^2} - U_{i+1}^{o^2}] .$$

This may be non-dimensionalized to give

$$P_{i+1}^o - P_i^i = \frac{\theta_{i+1}}{2} [U_i^{i^2} - U_{i+1}^{o^2}] . \quad (4-A)$$

Using the equation of state,  $\rho = \frac{p}{RT}$ , and assumption 3, the following equation is obtained:

$$\frac{\rho_i}{\rho_o} = \frac{T_o}{T_i} ,$$

or non-dimensionalized,

$$\theta_i = \frac{\theta_o}{\theta_i} . \quad (5-A)$$

Also, as used before

$$T_i = T_w - (T_w - T_o) e^{\frac{-2fx}{D}}$$

or non-dimensionalized,

$$\theta_1 = 1 - \bar{a} e^{-2\beta F_1 y} \quad (6-A)$$

where

$$\bar{a} = 1 - \theta_0.$$

An extremely important relationship may be obtained by combining equations (3-A) and (4-A),

$$U_{i+1}^0 = \frac{1}{1 + \frac{\Delta y}{2}} \left\{ U_i^1 - \sqrt{\frac{\Delta y^4}{4} U_i^{12} + 2 \Delta y^2 \left( 1 + \frac{\Delta y^2}{2} \right) \frac{P_i^1}{\theta_{i+1}}} \right\}. \quad (7-A)$$

Also, the continuity equation may be applied to a closed section of the manifold to yield  $\rho u = \text{constant}$  or

$$\theta_{i+1} U_i^1 = \theta_i U_i^0. \quad (8-A)$$

The problem may now be solved once the boundary conditions are established. These conditions are

$$\text{for } y = 0: \quad U_0^0 = \theta_0 = 1, \quad P_0^0 = \frac{M_0^2}{2}, \quad \theta = \theta_0,$$

$$\text{and } F = F_0.$$

With these boundary conditions, the problem may now be solved by using equations (6-A), (5-A), (8-A), (2-A), (1-A), (7-A) and (4-A), proceeding



in a cyclic manner until  $U = 0$ .

Equations for the Continuous Blowing Manifolds.--The differential equations, which describe the flow from a continuous blowing manifold, may be obtained by letting  $\Delta y$  approach zero as a limit. First by adding equations (1-A) and (4-A), and taking the limit as  $\Delta y \rightarrow 0$  (see Appendix I), the following results are obtained:

$$\frac{dP}{dy} + \frac{1}{2} \frac{d}{dy} (\rho U^2) + (\rho U^2) \left( \frac{F}{1-\bar{a}} \right) = 0. \quad (1-B)$$

Next equation (3-A) becomes

$$\frac{dU}{dy} = - \sqrt{\frac{2P}{\rho}}. \quad (2-B)$$

Solving equation (2-B)

$$P = \frac{\rho}{2} \left[ \frac{dU}{dy} \right]^2 \quad \text{and}$$

$$\frac{dP}{dy} = \rho \frac{dU}{dy} \frac{d^2U}{dy^2} + \frac{1}{2} \left[ \frac{dU}{dy} \right]^2 \frac{d\rho}{dy}. \quad (3-B)$$

The combination of equations (1-B) and (3-B) yields,

$$\rho \frac{dU}{dy} \frac{d^2U}{dy^2} + \frac{1}{2} \left[ \frac{dU}{dy} \right]^2 \frac{d\rho}{dy} + \frac{1}{2} \frac{d(\rho U^2)}{dy} + (\rho U^2) \left( \frac{F}{1-\bar{a}} \right) = 0. \quad (4-B)$$

Expanding  $\frac{d(\rho U^2)}{dy}$ ,

$$\frac{d(\varnothing^2)}{dy} = 2 \varnothing U \frac{dU}{dy} + U^2 \frac{d\varnothing}{dy} ,$$

now using equation (5-A),

$$\varnothing = \frac{\varnothing_o}{\varnothing} ; \quad \frac{d\varnothing}{dy} = - \frac{\varnothing_o}{\varnothing^2} \frac{d\varnothing}{dy}$$

and using equation (6-A)

$$\varnothing = 1 - \bar{a} e^{-2\beta_F y}; \quad \frac{d\varnothing}{dy} = 2\beta_F \bar{a} e^{-2\beta_F y} .$$

Combining all of these with equation (4-B) yields,

$$\left[ \frac{d^2 U}{dy^2} \right] \left[ \frac{dU}{dy} \right] + U \frac{dU}{dy} + \frac{U^2 F}{1-\bar{a}} - \frac{1}{2} \left\{ U^2 + \left[ \frac{dU}{dy} \right]^2 \right\} \left\{ \frac{2\beta_F \bar{a} e^{-2\beta_F y}}{1-\bar{a} e^{-2\beta_F y}} \right\} = 0 \quad (5-B)$$

The solution to the problem is then the solution of equation (5-B) with the following boundary conditions at  $y = 0$ :

$$U = 1, \quad \frac{dU}{dy} = -M_o \quad \text{and} \quad \bar{a} = 1 - \varnothing_o .$$

The friction factor,  $f$ , and consequently  $F$ , is a function of the Reynolds number, such that,

$$F_i = F_o \left( \frac{Re_i}{Re_o} \right)^N ,$$

If the absolute viscosity,  $\mu$ , is assumed to be a function of the absolute temperature such that  $\frac{\mu}{\mu_o} = C \left( \frac{T}{T_o} \right)$  where  $\mu_o$  is the absolute viscosity at a reference temperature  $T_o$ , then

$$F = F_o \left[ \frac{\rho U \theta_o}{C \theta} \right]^N \quad (6-B)$$

For air, C has a value of 1.08 over a temperature range of 100° F to 300° F. Also for laminar flow  $N = -1$  and for turbulent flow  $N = -1/4$ .

When it is deemed desirable to consider the variation of F with Reynolds number, an adjustment must be made in  $\theta$  and  $\frac{d\theta}{dy}$  as well as substituting equation (6-B) into equation (4-B). Beginning with Reynolds analogy,

$$\frac{dT}{T_w - T} = \frac{2f \, dx}{D} \quad ,$$

and non-dimensionalizing, then

$$\frac{d\theta}{dy} = 2\beta F (1-\theta) \quad (7-B)$$

With the use of equations (5-A) and (6-B), equation (7-B) becomes

$$\frac{d\theta}{dy} = 2\beta F_o \left[ \left( \frac{\theta_o}{\theta} \right)^2 \frac{U}{C} \right]^N (1-\theta) \quad (8-B)$$

Now equation (5-B) may be written as

$$\left[ \frac{d^2 U}{dy^2} \right] \left[ \frac{dU}{dy} \right] + U \frac{dU}{dy} + \frac{F_o \left( \frac{\Theta_o}{\Theta} \right)^{2N} (U)^{2+N}}{c^N (1-\bar{a})} \quad (9-B)$$

$$-\frac{1}{2} \left\{ U^2 + \left[ \frac{dU}{dy} \right]^2 \right\} \left\{ \frac{1}{\Theta} \frac{d\Theta}{dy} \right\} = 0.$$

Equations (8-B) and (9-B) may be solved simultaneously with the same boundary conditions as equation (5-B).

## CHAPTER III

## SOLUTIONS OF THE MATHEMATICAL EQUATIONS

The solution of the mathematical equations was, in all cases, carried out on a Burroughs 220 Computer. The programs were prepared with aid of a General Algol Program.

The analytical data presented in this paper were obtained from solutions of the equations for the continuous blowing manifolds. These solutions were chosen for presentation since they eliminate  $\Delta y$  as one of the variables. This reduction in the number of variables was most helpful when the data were presented graphically.

All the analytical data were obtained from numerical solutions of the mathematical equations. The equations for the discrete blowing manifold were by their nature very adaptable to a numerical solution. They were placed in correct order and then translated into the Algol language. The solutions of the equations for the continuous blowing manifold were solved numerically by the use of a Fourth Order Runge-Kutta.

The Runge-Kutta method is applicable only to first order differential equations. Equation (9-B) can be solved only after a change of variables has been made, so let

$$Z = \frac{dU}{dy} \quad \text{and} \quad \frac{dZ}{dy} = \frac{d^2U}{dy^2} .$$

Then equation (9-B) becomes

$$Z \frac{dZ}{dy} + UZ + C_1 \frac{U^{2+N}}{\Theta^{2N}} - \left[ \frac{U^2 + Z^2}{2\Theta} \right] \frac{d\Theta}{dy} = 0. \quad (1-C)$$

Solving (1-C) for  $\frac{dZ}{dy}$ ,

$$\frac{dZ}{dy} = - \left\{ U + \frac{C_1 U^{2+N}}{Z \Theta^{2N}} - \left[ \frac{U^2 + Z^2}{2\Theta Z} \right] \frac{d\Theta}{dy} \right\}. \quad (2-C)$$

Two other relationships are available

$$\frac{dU}{dy} = Z, \quad (3-C)$$

and from (8-B)

$$\frac{d\Theta}{dy} = C_2 \frac{U^N (1-\Theta)}{\Theta^{2N}}, \quad (4-C)$$

where

$$C_1 = \frac{F_o \Theta_o^{2N}}{C^N (1-\bar{a})}$$

and

$$C_2 = \frac{2\beta F_o \Theta_o^{2N}}{C^N}.$$

Equations (2-C), (3-C), and (4-C) now constitute a series of three first order differential equations which may be solved by use of the Runge-Kutta Method.

The general form for a Fourth Order Runge-Kutta, solving three simultaneous equations, is as follows:

for

$$\frac{d\Theta}{dy} = f_1 (y, U, Z, \Theta)$$

$$\frac{dU}{dy} = f_2 (y, U, Z, \Theta)$$

$$\frac{dZ}{dy} = f_3 (y, U, Z, \Theta) ,$$

then

$$\Theta_{n+1} = \Theta_n + \frac{1}{6} (J_1 + 2J_2 + 2J_3 + J_4)$$

$$U_{n+1} = U_n + \frac{1}{6} (K_1 + 2K_2 + 2K_3 + K_4)$$

$$Z_{n+1} = Z_n + \frac{1}{6} (L_1 + 2L_2 + 2L_3 + L_4)$$

where

$$J_1 = hf_1 (y_n, U_n, Z_n, \Theta_n)$$

$$J_2 = hf_1 (y_n + \frac{1}{2}h, U_n + \frac{1}{2}K_1, Z_n + \frac{1}{2}L_1, \Theta_n + \frac{1}{2}J_1)$$

$$J_3 = hf_1 (y_n + \frac{1}{2}h, U_n + \frac{1}{2}K_2, Z_n + \frac{1}{2}L_2, \Theta_n + \frac{1}{2}J_2)$$

$$J_4 = hf_1 (y_n + h, U_n + K_3, Z_n + L_3, \Theta_n + J_3) ,$$

and where  $h = \Delta y$ , the increment taken on  $y$ .

Likewise,

$$K_1 = hf_2 (y_n, U_n, Z_n, \Theta_n)$$

$$K_2 = hf_2 (y_n + \frac{1}{2} h, U_n + \frac{1}{2} K_1, Z_n + \frac{1}{2} L_1, \Theta_n + \frac{1}{2} J_1)$$

$$K_3 = hf_2 (y_n + \frac{1}{2} h, U_n + \frac{1}{2} K_2, Z_n + \frac{1}{2} L_2, \Theta_n + \frac{1}{2} J_2)$$

$$K_4 = hf_2 (y_n + h, U_n + K_3, Z_n + L_3, \Theta_n + J_3) \quad ,$$

and

$$L_1 = hf_3 (y_n, U_n, Z_n, \Theta_n)$$

$$L_2 = hf_3 (y_n + \frac{1}{2} h, U_n + \frac{1}{2} K_1, Z_n + \frac{1}{2} L_1, \Theta_n + \frac{1}{2} J_1)$$

$$L_3 = hf_3 (y_n + \frac{1}{2} h, U_n + \frac{1}{2} K_2, Z_n + \frac{1}{2} L_2, \Theta_n + \frac{1}{2} J_2)$$

$$L_4 = hf_3 (y_n + h, U_n + K_3, Z_n + L_3, \Theta_n + J_3)$$

The general form is simplified in this case since

$$\frac{d\Theta}{dy} = f_1 (U_n, \Theta_n),$$

$$\frac{dU}{dy} = f_2 (Z_n),$$

and

$$\frac{dZ}{dy} = f_3 (U_n, Z_n, \Theta_n) \quad .$$

The solutions of these equations for the continuous blowing manifold



were carried out by use of an Algol Program. The only variable involved, other than the boundary conditions, was  $h$ . The proper value for  $h$  was determined by computing several solutions, the value of  $h$  being the parameter which was changed. The largest value of  $h$  was chosen, which would produce an identical solution, to six significant figures, with another solution using a smaller value of  $h$ . This value of  $h$  was found to be 0.05.

## CHAPTER IV

## EQUIPMENT

Inlet Air.--The inlet air was supplied by a multistage centrifugal blower with a maximum capacity of 200 cfm of free air at a pressure of 30 inches of water. The flow of air was controlled by two throttling valves. A 2-inch gate valve was placed on the inlet side of the blower. The air was then carried by a 2-inch iron pipe line to the gas meter. A 1-inch gate valve preceded the gas meter.

The air flow was measured with a dry gas meter which was calibrated by the Atlanta Gas Light Company (a smaller meter was used when the pitot tubes were calibrated). The inlet pressure to the meter was measured with a "U" tube manometer, while the inlet temperature was measured with an iron-constantan thermocouple.

The air was then carried from the gas meter to the test section, first by a 2-inch iron pipe line and second by a 3/4-inch copper tube. The total length of the 2-inch pipe line was 25 feet. The air was carried through an elbow into the 3/4-inch copper tube. This tube (the same type of tubing as was used on the manifold) was 6 feet long, which allowed for fully developed turbulent flow at the entrance to the test section. To minimize the transfer of heat from the test section to the inlet air, the inlet section of tubing was connected to the manifold by a piece of rubber tubing.

Test Section.--The heated manifold consisted of a 3/4-inch copper tube (0.795 inch I.D.) 44 inches long with ten equally spaced ports (0.235 inch diameter) 4 inches on centers, and 4 inches of tubing before and after the ports (see Figure 3). The port (see Figure 4) was constructed by drilling a 0.235 inch diameter hole in the copper tube. A brass tee, bored to fit, was slipped over the tubing and then soldered in position over the port. The downstream end of the manifold was closed with a gate valve.

The port section (see Figures 4,5) was then completed by connecting a nylon tube into the tee and allowing the air to pass through the wall of the steam jacket. The nylon tube consisted of 3/8-inch and a 5/16-inch (0.235 inch I.D.) nylon tube, one placed inside the other, to minimize the effect of heat transfer upon the flow of the air as it passed through the port. The total length of the nylon tubes was 12 inches.

Steam Jacket.--A steam jacket was utilized to provide an isothermal wall for the heated runs. The jacket consisted of a 6-inch black iron pipe, capped at both ends (see Figure 3). Holes were drilled in both ends and along one side to allow for the entrance of the manifold. The openings were sealed by use of rubber stoppers, cut to fit over the manifold.

The jacket was operated at atmospheric pressure or slightly less. This was accomplished by use of throttling valves on the steam line and on the drain. The condensate (sometimes steam) was drained from the jacket into an ejector which consisted of a spray nozzle and the appropriate control valves. The ejector was necessary to insure the maintenance of a vacuum in the steam jacket. It was necessary to maintain a pressure close

to atmospheric so that the rubber stoppers would maintain a tight seal. As an aid in maintaining the pressure, a pressure tap was provided to connect the steam jacket to a "U" tube manometer.

Pitot Tubes.--The pitot tubes were constructed from stainless steel hypodermic tubing and copper tubing. A 4-inch piece of 20 gage hypodermic tubing was cut and inserted about 1 inch inside a 6-inch piece of 1/4-inch copper tubing (see Figure 5). The joint was sealed with silver solder. Three small wire supports, for centering the pitot tube, and an iron-constantan thermocouple were soldered to the stainless steel tube.

The copper tubing was used in the construction of the pitot tube for two reasons. First, it was needed to provide a rigid support for the stainless steel tubing and, secondly, it was needed to connect the rubber tubing to the manometer, since rubber tubing as small as the pitot tube would cause a large time delay.

Manometers.--All pressure measurements, except the barometric pressure, were made with manometers. In each case the head was given in inches of water. Three "U" tube manometers were used for the measurements of the pressure at the dry gas meter, at the inlet to the heated manifold, and in the steam jacket. The manometer for the steam jacket was provided simply as a safety measure.

The critical measurements were the total pressures in the discharge tubes. The total head (see Appendix II) was measured with a micromanometer with subdivisions of 0.001 inches (see Figure 6). The micromanometer was connected to a small manifold (see Figure 7). Each pitot tube was also connected to this manifold by a rubber tube which was sealed by

a spring cutoff. Only one cutoff at a time was opened, allowing a quick and direct connection between the pitot tube and the micromonometer.

Thermocouples.--The temperature measurements were performed with 26 gage iron-constantan thermocouples. The thermocouple emf's were measured with a portable potentiometer using an ice bath as the cold junction. The connections of the thermocouples were handled through a 20-position junction box.

Thermocouples were attached to each pitot tube, at the gas meter, at the inlet to the manifold, and to the wall of the manifold, inside the steam jacket. The cold junction was formed in an ice bath, which was maintained in a vacuum bottle.



## CHAPTER V

## TEST PROCEDURE

The test procedure required several steps before the flow distribution could be measured. These steps were: verification of the thermocouples, measuring of the friction factor  $F$ , and calibration of the pitot tubes.

Thermocouples.--The validity of the thermocouples could be established either by calibrating them or by checking them against a standard. It was decided to check first against a standard. Since this check was satisfactory, no further action was necessary. A check was made against two standards with all of the thermocouples indicating the same emf measured to 0.01 mv, and also matching the standards. The two cases were: first, a water bath whose temperature was measured with a thermometer bearing a Bureau of Standards calibration and, second, a steam bath at atmospheric pressure.

Friction Factor.--It was necessary to consider the friction factor, since the flow distribution depends upon it. A rubber tube connected the first and last ports to opposite sides of the micromonometer for measuring the pressure drop. Those ports became pressure taps, the other ports were closed. The gate valve at the end of the manifold was opened, the centrifugal blower was started, the air flow was adjusted and allowed to reach equilibrium.

The air flow was adjusted for five different flow rates. During these runs, measurements were made and recorded. These measurements were: static pressure at the gas meter, static pressure drop in the tube, barometric pressure, temperature at the gas meter, manifold inlet temperature, wet and dry bulb temperatures and the time required for ten cubic feet of air to pass through the gas meter.

Calibrate Pitot Tubes.--The calibration of the pitot tubes began with the connection into the supply line of a small dry gas meter. The meter normally used was too large for the measurement of the flow through one port. The pitot tube to be calibrated was positioned, the remaining ports were closed, and the valve at the end of the manifold was closed so all of the air passing through the gas meter passed through the port. This was done for each pitot tube.

The blower was started, and the air flow was adjusted and allowed to reach an equilibrium. The following measurements were then made and recorded: The pitot head in inches of water, static pressure at the meter, barometric pressure, temperature of the discharge air, temperature at the meter, wet and dry bulb temperatures, and the time required for one cubic foot of air to pass through the gas meter.

Flow Distribution.--The data for flow distribution was obtained first by positioning the pitot tubes. Runs were made with five, seven, and ten ports open. With the pitot tubes in place, the remaining ports were closed, the air flow was adjusted and allowed to reach an equilibrium. The air flow was adjusted so as to match heated and non-heated runs, that is the total mass flow was the same for a pair of runs, one heated and

the other not heated. When heat was used, the air flow was adjusted first, the steam valve was opened and finally the ejector valves were opened. The steam inlet valve and the ejector valves were opened. The steam inlet valve and the ejector valves were adjusted until steady state was reached, then a final adjustment was made on the air flow.

Once the final adjustment was made and equilibrium reached, only minor adjustments were necessary to maintain equilibrium in the steam jacket. These adjustments were made during the run. The following measurements were made and recorded: the head at each pitot tube, inlet static pressure, static pressure at the gas meter, barometric pressure, inlet temperature, outlet temperature for each port, temperature at the meter, wall temperature of manifold, wet and dry bulb temperatures, and the time required for ten cubic feet of air to pass through the gas meter.



## CHAPTER VI

## ANALYSIS OF RESULTS

Mathematical Equations.--The results of the calculations outlined in Chapter III appear in Figures 9 through 28. The figures may be broken into five groups.

First, Figures 9 through 17 show  $\frac{dw}{dy}$  vs.  $y$ . In these figures,

$$\frac{dw}{dy} = \frac{-\frac{d(\phi U)}{dy}}{-\frac{d(\phi U)}{dy}} \bigg|_{y=0}$$

where

$$-\frac{d(\phi U)}{dy} = \frac{\text{Side flow rate}}{\text{Total flow}} ,$$

and  $y$  is the dimensionless distance which has already been defined. The area under the curves,  $A_c$ , is

$$A_c = \int \frac{dw}{dy} dy = \frac{\int \frac{d(\phi U)}{dy} dy}{\frac{d(\phi U)}{dy}} \bigg|_{y=0} .$$

The side flow may be obtained as a percentage of the total flow by multiplying  $A_c$  by  $-\frac{d(\phi U)}{dy} \bigg|_{y=0}$ , which comes from Figures 23 through 25.

The figures show for larger values of the parameter  $M_o$ , the flow is more uniform than for small values of  $M_o$ . When  $M_o$  is large, the other parameters have little effect on the flow distribution. This may be explained by looking at  $M_o$ . Now

$$M_o^2 = \frac{p_o - p_s}{\rho_o u_o^2} ,$$

and thus when  $M_o$  is large, either  $(p_o - p_s)$  is large or  $(\rho_o u_o^2)$  is small, this means the bleed off rate is large compared to the pressure rise due to a reduction in  $u$  or a pressure drop in the manifold. That is to say, the manifold acts like a large reservoir with a number of openings and each port has essentially the same pressure differential acting across it. When  $M_o$  is small, the pressure rises and drops are the predominate factors. This results in an uneven flow distribution with an increase in the initial side flow rates. The effects of heating are much greater when  $M_o$  is small.

Second, Figures 18 through 19 show  $w$  vs.  $y$  for various values of  $\Delta y$ . These curves show the relationship between the solutions obtained from the differential equations and those obtained from the finite equations. The smaller the value of  $\Delta y$ , the nearer the two solutions will compare, and the smoother the flow distribution.

Third, Figures 20 through 22 show  $\frac{\text{Range in side flow rate}}{\text{Initial side flow rate}}$  vs  $M_o$ .

These curves give the maximum variation as a percentage of the initial side flow rate. When  $M_o$  is small, the variation is greatest and increases

when heating is applied. However, when  $M_o$  is large, the variations become small and in the limit, approach zero.

Fourth, Figures 23 through 25 present  $\frac{\text{Initial side flow rate}}{\text{Total flow}}$  vs  $M_o$ .

These curves show a linear variation with  $M_o$ . When  $\phi_o$  equals unity,  $F_o$  has no effect on the relationship; but when heating is applied, as  $F_o$  increases the initial side flow rate increases.

Fifth, Figures 26 through 28 show the dimensionless length  $L'$ , where  $L' = 4\alpha K \sqrt{2\beta'} \frac{L}{D}$ , vs.  $M_o$ . These curves reveal little or no effect from heating. As the friction increases so does the length  $L'$ . This indicates that as the friction losses become large they counteract the pressure recovery as  $U$  is reduced and heat is added; the result is that the manifold pressure drops requiring a greater discharge area for the same flow rate.

Heating causes the curves to cross, which indicates that the effects are reversed as  $M_o$  becomes smaller. That is, the pressure rises due to thermal energy input and reductions in  $U$  are larger than the pressure losses due to friction.

Experimental Data.--The Figures 29 through 38 show the correlation curves for the experimental data. The curves were obtained by drawing a smooth curve which was positioned so the scattering of data was balanced above and below the curve. These curves show a normal scattering of data.

The data were obtained from computed mass flow rates. The experimental data began with the measurement of the head from the pitot tubes along with the temperature at each port and the total pressure. The Reynolds number in the port could be obtained from the calibration curve

for the pitot tube. The temperature and atmospheric pressure were sufficient to determine the kinematic viscosity. This then gave the volume flow rate.

From the volume flow rate, the mass flow rate could be computed when the specific volume was known. The wet and dry bulb temperatures were obtained as a part of the experimental data. They allowed, along with the barometric pressure, the specific volume to be read from a psychrometric chart. The mass flow rate was then obtained.

The mass flow from each port was summed and compared with the mass flow obtained from the gas meter. Any difference was corrected, applying the correction equally to the flow from each port. The data which appear in Figures 29 through 38 then represent the ratio of the flow from a port divided by the flow from the first port.

The Figures 39 through 48 compare the correlation curves with the solutions from the finite equations. They compare favorably with a slight separation at the end. The measured flow is less at the end of the manifold than the predicted flow. Some of the computed curves stop short of the actual number of ports. This occurred because the solutions of the equations begin with a specified set of initial conditions. These conditions may not completely fit all of the conditions downstream. The starting values were computed from the experimental data. There was apparently enough error in the initial conditions to prevent a complete matching of the downstream conditions.



## CHAPTER VII

## CONCLUSIONS AND RECOMMENDATIONS

Conclusions.--In the design of a manifold system, whether heated or unheated, it is desirable to make  $M_0$  as large as possible. This will make the variation in the mass flow rate as small as possible. The  $\frac{L}{D}$  ratio should be kept as small as possible since this allows the manifold to act as a large reservoir thus providing a more uniform distribution.

The transfer of heat to the gas will in all cases add to the difficulties of maintaining a uniform distribution. Heat transfer should be minimized whenever possible. The faster the fluid is removed from the manifold, the less heat may be transferred. This is accomplished by keeping  $M_0$  high and  $F_0$  low.

The value of  $F_0$  should not, in all cases, be kept necessarily low. It will be noted that for certain values of the parameters, a higher value of  $F_0$  will allow for a more uniform flow distribution. In these cases it is, of course, desirable to attempt to attain this value of  $F_0$ . It is not always possible to obtain the desired values to give a uniform flow distribution but the alternatives can at least be investigated.

Recommendations.--For the advancement of this study, further investigations should be made for additional cases along this same line.

1. Further experiments should be performed with a series of manifold systems in an endeavor to examine the flow distribution in the region

of greatest deviation so the effect of heating might be more pronounced. This would allow for a more conclusive verification of the equations used in this paper.

2. Further data should be obtained to give a wider range of data and to help further establish the shape of some of the curves for  $M_0$  less than unity and greater than three.

3. Additional physical configurations should be studied; for example, a non-uniform cross section for the manifold or ports at an angle other than 90 degrees to the axis of the system.

4. The case of a sucking manifold should be investigated. This could then be tied into the blowing manifold solution by joining the two manifolds with tubes which would replace the ports in each case.

The final recommendation would, in all likelihood, be the most useful of all the solutions. This would then very closely resemble mathematically some physical applications.

## APPENDIX

## APPENDIX I

## THE DIFFERENTIAL EQUATIONS

The differential equations which describe the flow from a continuous blowing manifold may be obtained by letting  $\Delta y$  approach zero as a limit. Before a limit may be taken, the finite difference equations must be written from the beginning of one port to the beginning of the next port. This involves the equations which describe the flow through the straight portion of the tube plus those equations which describe the flow past the port.

Start with equations (1-A), (2-A), and (4-A),

$$P_{i+1}^i - P_i = -\phi_i U_i^o \frac{(U_i^o + U_i^i)}{2} \left[ F_i \Delta y + G_i \right] \quad (1-A)$$

$$G_i = \frac{1}{2\phi} \ln \frac{Q_{i+1}}{Q_i} \quad (2-A)$$

$$P_{i+1}^o - P_i^i = \frac{\phi_{i+1}}{2} \left[ U_i^{i^2} - U_{i+1}^{o^2} \right] \quad (4-A)$$

When assumption two is applied,

$$\phi_{i+1} \left[ U_i^{i^2} - U_{i+1}^{o^2} \right] = (\phi U^2)_i^i - (\phi U^2)_{i+1}^o ,$$



equation (4-A) becomes

$$P_{i+1}^o - P_i^o = \frac{1}{2} \left[ (\varnothing U^2)_i^o - (\varnothing U^2)_{i+1}^o \right] . \quad (1-D)$$

Now when equations (1-A) and (4-D) are added,

$$P_{i+1}^o - P_i^o = - (\varnothing U)_i^o \left( \frac{U_i^o + U_i^i}{2} \right) \left[ F_i \Delta y + G_i \right] - \frac{1}{2} \left[ (\varnothing U^2)_{i+1}^o - (\varnothing U^2)_i^o \right] . \quad (2-D)$$

Beginning with equation (8-A),

$$\varnothing_{i+1} U_i^i = \varnothing_i U_i^o , \quad (8-A)$$

an interesting relationship may be obtained,

$$(\varnothing U^2)_i^i - (\varnothing U^2)_i^o = \varnothing_{i+1} U_i^{i^2} - \varnothing_i U_i^{o^2} .$$

Now using (8-A)

$$\varnothing_{i+1} U_i^{i^2} = \varnothing_i U_i^o U_i^i$$

also

$$U_i^i = \frac{\varnothing_i}{\varnothing_{i+1}} U_i^o \quad (3-D)$$

then

$$\varnothing_{i+1} U_i^{i^2} = \frac{(\varnothing_i U_i^o)^2}{\varnothing_{i+1}} ,$$

this then yields

$$(\varnothing U^2)_i^i - (\varnothing U^2)_i^o = (\varnothing_i U_i^o)^2 \left[ \frac{1}{\varnothing_{i+1}} - \frac{1}{\varnothing_i} \right] .$$

Finally the needed relationship is obtained,

$$(\varnothing U^2)_i^i = (\varnothing U^2)_i^o + (\varnothing U)_i^{o2} \left[ \frac{1}{\varnothing_{i+1}} - \frac{1}{\varnothing_i} \right] . \quad (4-D)$$

Equation (4-D) also gives another useful relationship,

$$U_i^i = \left\{ \frac{\varnothing_i}{\varnothing_{i+1}} U_i^{o2} + \frac{(\varnothing U)_i^{o2}}{\varnothing_{i+1}} \left[ \frac{1}{\varnothing_{i+1}} - \frac{1}{\varnothing_i} \right] \right\}^{1/2} . \quad (5-D)$$

Substituting (4-D) and (5-D) into (2-D), the following is obtained:

$$\begin{aligned} \frac{P_{i+1} - P_i}{\Delta y} &= -(\varnothing U)_i^o \left( \frac{U_i^o}{2} + \frac{1}{2} \left\{ \frac{\varnothing_i}{\varnothing_{i+1}} U_i^{o2} + \frac{(\varnothing U)_i^{o2}}{\varnothing_{i+1}} \right. \right. \\ &\quad \left. \left. \left[ \frac{1}{\varnothing_{i+1}} - \frac{1}{\varnothing_i} \right] \right\}^{1/2} \right) \left[ F_i + \frac{G_i}{\Delta y} \right] - \frac{1}{2 \Delta y} \left\{ (\varnothing U^2)_{i+1}^o \right. \\ &\quad \left. - (\varnothing U^2)_i^o - (\varnothing U)_i^{o2} \left[ \frac{1}{\varnothing_{i+1}} - \frac{1}{\varnothing_i} \right] \right\} . \end{aligned} \quad (6-D)$$

Equation (6-D) is in the proper form to take a limit. Taking a limit as  $\Delta y$  approaches zero: as  $\Delta y \rightarrow 0$ ,

$$\phi_{i+1} \rightarrow \phi_i ;$$

$$\lim_{\Delta y \rightarrow 0} \frac{P_{i+1}^O - P_i^O}{\Delta y} = \frac{dP}{dy} ;$$

$$\lim_{\Delta y \rightarrow 0} \frac{\phi_{i+1} - \phi_i}{\phi_i} = \frac{\phi}{\phi} = 1 ;$$

$$\lim_{\Delta y \rightarrow 0} \left( \frac{1}{\phi_{i+1}} - \frac{1}{\phi_i} \right) = \left( \frac{1}{\phi} - \frac{1}{\phi} \right) = 0 ;$$

$$\lim_{\Delta y \rightarrow 0} \frac{G_i}{\Delta y}, \text{ from equations (2-A) and (6-A)}$$

or

$$\frac{G_i}{\Delta y} = \frac{1}{2\beta \Delta y} \ln \left\{ \frac{1 - \bar{a} e^{-2\beta F_i \Delta y(i)}}{1 - \bar{a} e^{-2\beta F_i \Delta y(i-1)}} \right\}$$

$$\frac{G_i}{\Delta y} = \frac{\ln \left\{ 1 - \bar{a} e^{-2\beta F_i \Delta y(i)} \right\}}{2\beta \Delta y} - \frac{\ln \left\{ 1 - \bar{a} e^{-2\beta F_i \Delta y(i-1)} \right\}}{2\beta \Delta y}$$

In order to determine the limit of  $\frac{G_i}{\Delta y}$ , apply L' Hospital's rule differ-

entiating with respect to  $\Delta y$ ,

$$\lim_{\Delta y \rightarrow 0} \frac{G_i}{\Delta y} = \lim_{\Delta y \rightarrow 0} \left\{ \frac{2\beta F_i(i) \bar{a} e^{-2\beta F_i \Delta y(i)}}{2\beta [1 - \bar{a} e^{-2\beta F_i \Delta y(i)}]} \right. \\ \left. - \frac{2\beta F_i(i-1) \bar{a} e^{-2\beta F_i \Delta y(i-1)}}{2\beta [1 - \bar{a} e^{-2\beta F_i \Delta y(i-1)}]} \right\}$$

$$\begin{aligned}
&= \lim_{\Delta y \rightarrow 0} \left\{ \frac{\bar{a} F_i(i) e^{-2\beta F_i \Delta y(i)}}{1 - \bar{a} e^{-2\beta F_i \Delta y(i)}} - \frac{\bar{a} F_i(i-1) e^{-2\beta F_i \Delta y(i-1)}}{1 - \bar{a} e^{-2\beta F_i \Delta y(i-1)}} \right\} \\
&= \left\{ \frac{\bar{a} F_i(i) 1}{1 - \bar{a}(1)} - \frac{\bar{a} F_i(i-1)(1)}{1 - \bar{a}(1)} \right\} \\
&= \left\{ \frac{\bar{a} F_i(i) - \bar{a} F_i(i-1) + \bar{a} F_i}{1 - \bar{a}} \right\}
\end{aligned}$$

thus

$$\lim_{\Delta y \rightarrow 0} \frac{G_i}{\Delta y} = \frac{\bar{a} F}{1 - \bar{a}} ;$$

$$\begin{aligned}
&\lim_{\Delta y \rightarrow 0} \left\{ (\varnothing)_i^o \left[ \frac{U_i^o}{2} + \frac{1}{2} \left( \frac{\varnothing_i}{\varnothing_{i+1}} U_i^{o2} + \frac{(\varnothing)_i^{o2}}{\varnothing_{i+1}} \left( \frac{1}{\varnothing_{i+1}} - \frac{1}{\varnothing_i} \right) \right)^{1/2} \right] \right\} \\
&= \left\{ (\varnothing)_i^o \left[ \frac{U_i^o}{2} + \frac{1}{2} (U_i^{o2})^{1/2} \right] \right\} \\
&= \left\{ (\varnothing)_i^o [U_i^o] \right\} ,
\end{aligned}$$

then

$$\begin{aligned}
&\lim_{\Delta y \rightarrow 0} \left\{ (\varnothing)_i^o \left[ \frac{U_i^o}{2} + \frac{1}{2} \left( \frac{\varnothing_i}{\varnothing_{i+1}} U_i^{o2} + \frac{(\varnothing)_i^{o2}}{\varnothing_{i+1}} \left( \frac{1}{\varnothing_{i+1}} - \frac{1}{\varnothing_i} \right) \right)^{1/2} \right] \right\} \\
&= \varnothing^2 ;
\end{aligned}$$

$$\begin{aligned}
\lim_{\Delta y \rightarrow 0} \frac{1}{2 \Delta y} & \left\{ (\varrho U^2)_{i+1}^o - (\varrho U^2)_i^o - \varrho U_i^{o2} \left[ \frac{1}{\varrho_{i+1}} - \frac{1}{\varrho_i} \right] \right\} \\
&= \lim_{\Delta y \rightarrow 0} \frac{1}{2 \Delta y} \left\{ (\varrho U^2)_{i+1}^o - (\varrho U^2)_i^o \right\} = \frac{1}{2} \frac{d(\varrho U^2)}{dy} .
\end{aligned}$$

Substituting the above limits into equation (5-D), (5-D) becomes

$$\frac{dP}{dy} = -(\varrho U^2) \left( F + \frac{\bar{a} F}{1-\bar{a}} \right) - \frac{1}{2} \frac{d(\varrho U^2)}{dy}$$

or

$$\frac{dP}{dy} + \frac{1}{2} \frac{d(\varrho U^2)}{dy} + (\varrho U^2) \left( \frac{F}{1-\bar{a}} \right) = 0 \quad (7-D)$$

Likewise, beginning with equation (3-A),

$$U_{i+1}^o - U_i^o = -\Delta y \sqrt{\frac{P_{i+1}^o + P_i^o}{\varrho_{i+1}}} \quad (3-A)$$

and substituting (1-A) and (3-D) into (3-A) gives,

$$\frac{1}{\Delta y} \left\{ U_{i+1}^o - U_i^o \frac{\varrho_i}{\varrho_{i+1}} \right\} = - \left\{ \frac{P_{i+1}^o + P_i^o - \varrho_i U_i^o \frac{(U_i^o + U_i^o)}{2} [F_i \Delta y + G_i]}{\varrho_{i+1}} \right\}^{1/2} .$$

Now applying a limit,

$$\lim_{\Delta y \rightarrow 0} \frac{1}{\Delta y} \left\{ U_{i+1}^o - U_i^o \frac{\varrho_i}{\varrho_{i+1}} \right\} = \lim_{\Delta y \rightarrow 0} \frac{1}{\Delta y} \left\{ U_{i+1}^o - U_i^o \right\} = \frac{dU}{dy}$$

using equation (5-A),

then 
$$\frac{\phi_{i+1}}{\phi_i} = \frac{\phi_i}{\phi_{i+1}}$$

$$G_i = \frac{1}{2\beta} \ln \frac{\phi_i}{\phi_{i+1}},$$

hence

$$\lim_{\Delta y \rightarrow 0} G_i = \frac{1}{2\beta} \ln(1) = 0;$$

$$\lim_{\Delta y \rightarrow 0} F_i \Delta y = 0.$$

Therefore

$$\begin{aligned} \lim_{\Delta y \rightarrow 0} & \left\{ \frac{P_{i+1}^0 + P_i^0 - \phi_i U_i^0 \frac{(U_i^0 + U_{i+1}^0)}{2} [F_i \Delta y + G_i]}{\phi_{i+1}} \right\}^{1/2} \\ & = \left\{ \frac{2P}{\phi} \right\}^{1/2}. \end{aligned}$$

Finally, the desired relationship is obtained,

$$\frac{dU}{dy} = - \left\{ \frac{2P}{\phi} \right\}^{1/2}. \quad (8-D)$$

## APPENDIX II

## THE CALIBRATION AND CORRELATION OF THE PITOT TUBES

The calibration of the pitot tubes actually began with a mathematical analysis of the equations related to the pitot tube followed by an experimental verification of the results. For this particular application, the most convenient pressure differential to measure was the difference in the total pressure in the tube (see Figure 3) and the total pressure (barometric pressure) surrounding the tube. The barometric pressure was much easier to measure than the static pressure, since the plastic tube had a diameter of only 0.235 inches. The pitot tube was inserted into the plastic tube a sufficient distance to eliminate the exit effects.

The mathematical analysis begins by writing the equations for the pitot tube when the fluid is air. The equation for the total pressure at the point of the pitot tube is,

$$p_{ta} = p_{sa} + \frac{\rho_a v^2}{2}$$

or

$$p_{ta} - p_{sa} = \frac{\rho_a v^2}{2} \quad (1-E)$$

Now the pressure drop from the end of the pitot tube to the surroundings is



$$p_{sa} - p_{Ba} = \frac{f l}{D} \frac{\rho_a v^2}{2} \quad (2-E)$$

Adding equations (1-E) and (2-E), the desired pressure differential is obtained,

$$p_{ta} - p_{Ba} = \left( 1 + \frac{f l}{D} \right) \frac{\rho_a v^2}{2} \quad (3-E)$$

The pressure differential is more easily measured in terms of the head, so

$$h_a = \frac{p_{ta} - p_{Ba}}{\rho_a} = \left( 1 + \frac{f l}{D} \right) \frac{v^2}{2}$$

The head was measured in inches of water,

$$\text{so} \quad h_w = \frac{h_a \rho_a}{\rho_w}$$

$$\text{thus} \quad h_w = \frac{\left( 1 + \frac{f l}{D} \right) \rho_a v^2}{2 \rho_w} \quad (4-E)$$

Now if equation (4-E) is to be correlated, it must be non-dimensionalized,

$$h_w \frac{\rho_a D^2}{\mu_a^2} = \frac{\left( 1 + \frac{f l}{D} \right) \rho_a^2 v^2 D^2}{2 \rho_w \mu_a^2},$$

$$\text{or } \frac{h_w \rho_a D^2}{\mu_a^2} = \frac{\left(1 + \frac{f l}{D}\right)}{2 \rho_w} \text{Re}_a^2 .$$

If the absolute viscosity,  $\mu_a$ , is assumed to be a function of the absolute temperature such that  $\mu_a = C \mu_{oa} \left(\frac{T}{T_o}\right)$ , also from the equa-

tion of state,  $\rho_a \approx \frac{p}{RT}$ ,

then

$$\frac{\mu_a^2}{\rho_a} = \frac{C \mu_{oa}^2 T_o^3 R}{T_o^2 p} ,$$

$$\text{so } \frac{2 h_w p T_o^2 D^2}{C T_o^3 R \mu_{oa}^2} = \left(1 + \frac{f l}{D}\right) \text{Re}_a^2 .$$

$$\text{Let } C_1 = \left(1 + \frac{f l}{D}\right) \quad \text{and} \quad C_2 = \frac{2 T_o^2 D^2}{C R \mu_{oa}^2} ,$$

$$\text{then } \frac{h_w p}{T^3} = \frac{C_1}{C_2} \text{Re}_a^2 .$$

$$\text{Let } C_3 = \frac{C_1}{C_2}$$

$$\text{and finally } \frac{h_w p}{T^3} = C_3 \text{Re}_a^2 . \quad (5-E)$$

Equation (5-E) will then form a straight line when plotted on log-log

paper. Notice that  $\frac{h_w p}{T^3}$  is not dimensionless, however  $C_3$  (a constant) will contain the same quantities as  $\frac{h_w p}{T^3}$ .

Equation (5-E) was verified and the pitot tubes were made from hypodermic tubing with three spacers provided on each tube to assure the proper relocation of the pitot tube after its removal from the plastic tube. The calibration of the pitot tubes was a routine matter once the relocation of the tube was assured.

After the relocation of the pitot tubes was effected, equation (5-E) was easily verified. All but one of the ports were closed, then the total flow was measured with a dry gas meter, at the same time the head,  $h_w$ , the temperature,  $T$ , and the pressure,  $p$ , were measured. These data were collected for a range of the parameters,  $\frac{h_w p}{T^3}$  and  $Re_a$ . To further verify equation (5-E), data were collected for various values of  $h_w$  and  $T$ .

The correlation, as can be seen from Figure 8, was quite acceptable. Once equation (5-E) was verified, the pitot tubes were then calibrated by taking data for a range of Reynolds numbers and plotting  $\frac{h_w p}{T^3}$  versus  $Re_a$ . The reason data were taken for each pitot tube was the location of the pitot tube. Each tube was in a different position relative to its own plastic tube, thus  $C_3$  had a different value for each tube. The calibration curve for each pitot tube was then used to determine the mass flow rate through each port.

## APPENDIX III

### DATA

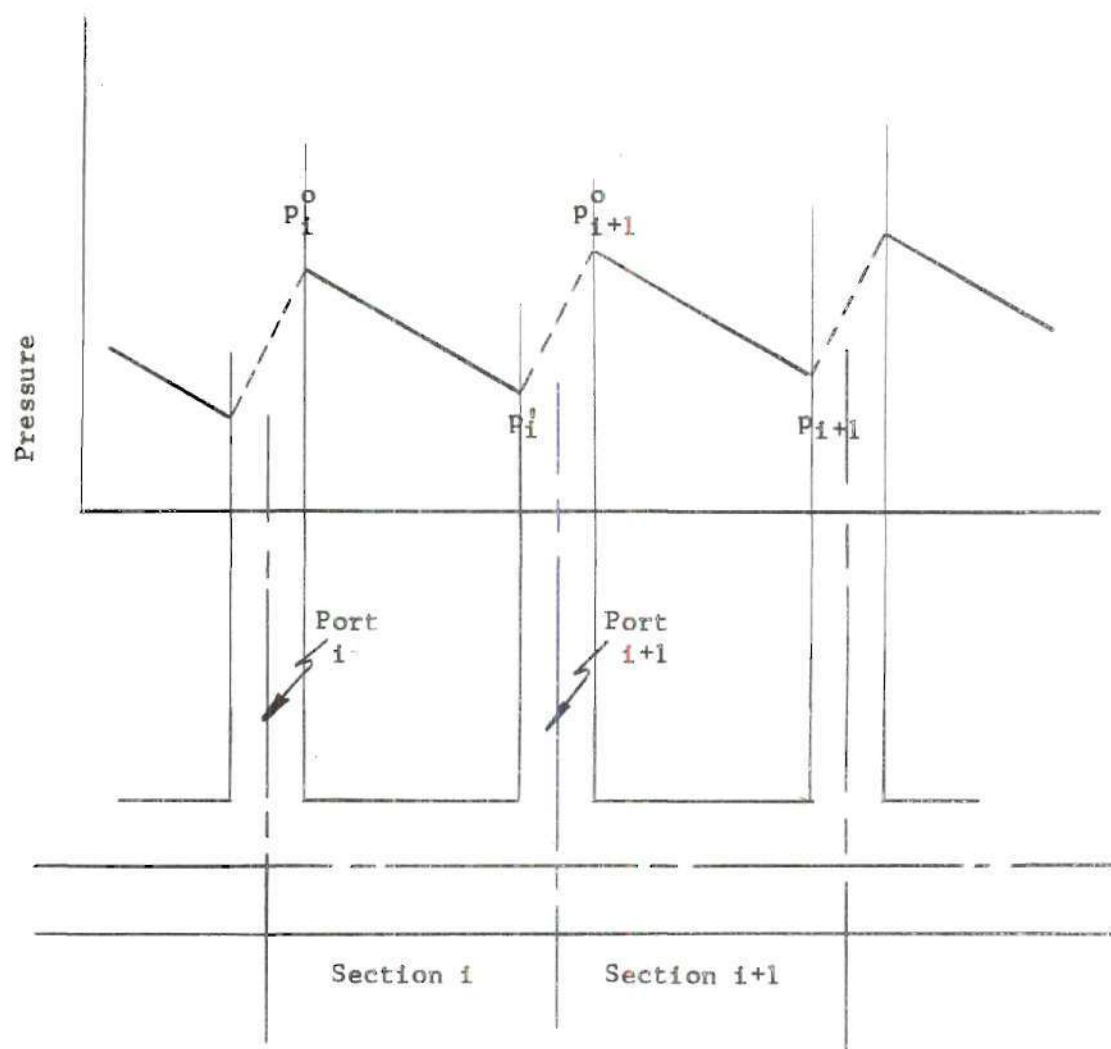


Figure 1. Nomenclature Use for One-dimensional Theory of Manifolds

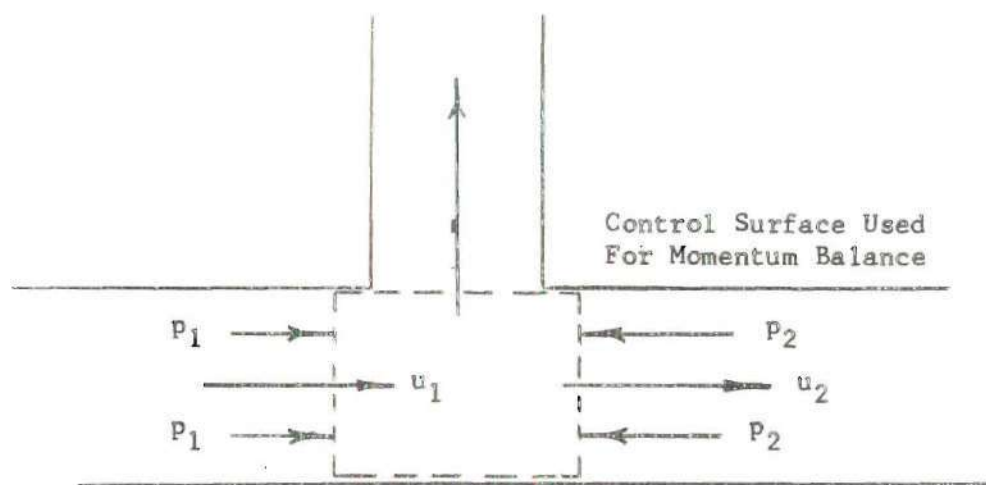


Figure 2. Fluid Pressures and Velocities  
Near a Manifold Port

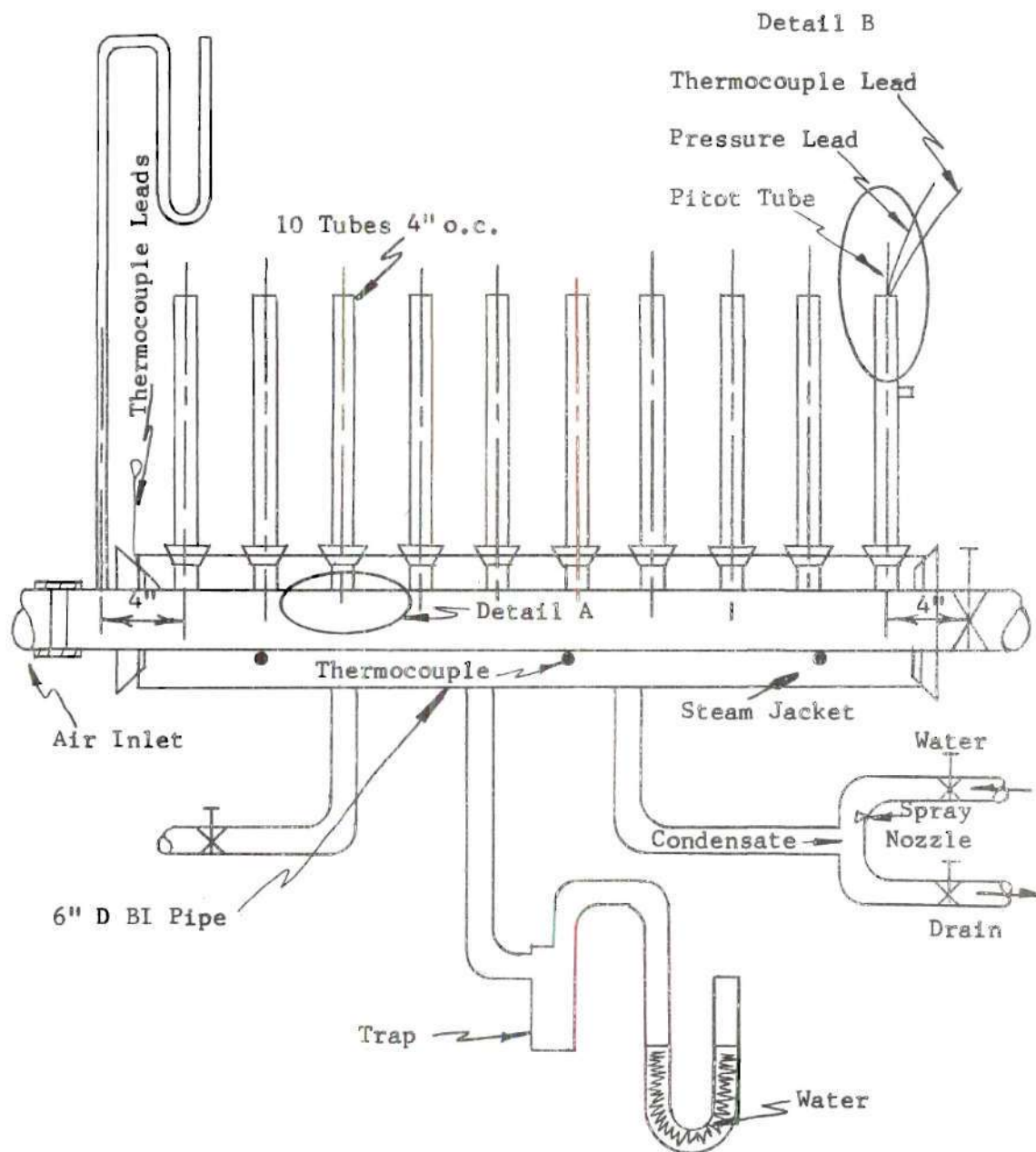
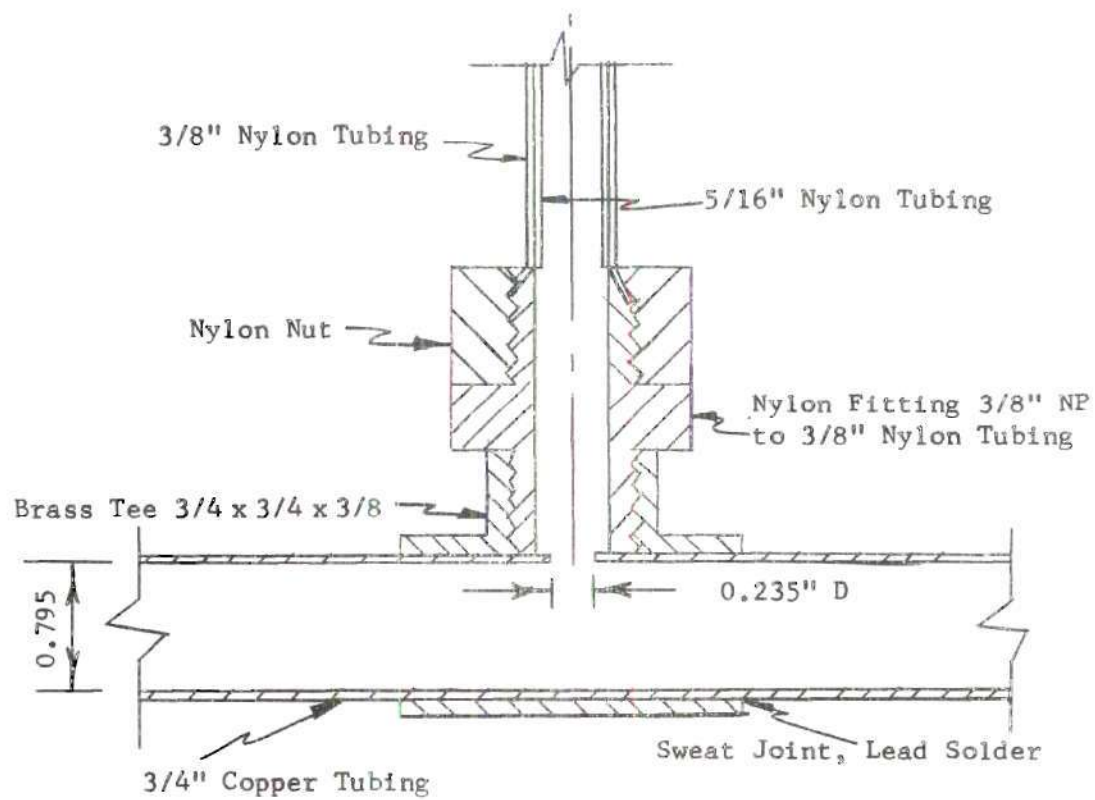


Figure 3. Schematic Diagram of Experimental Equipment

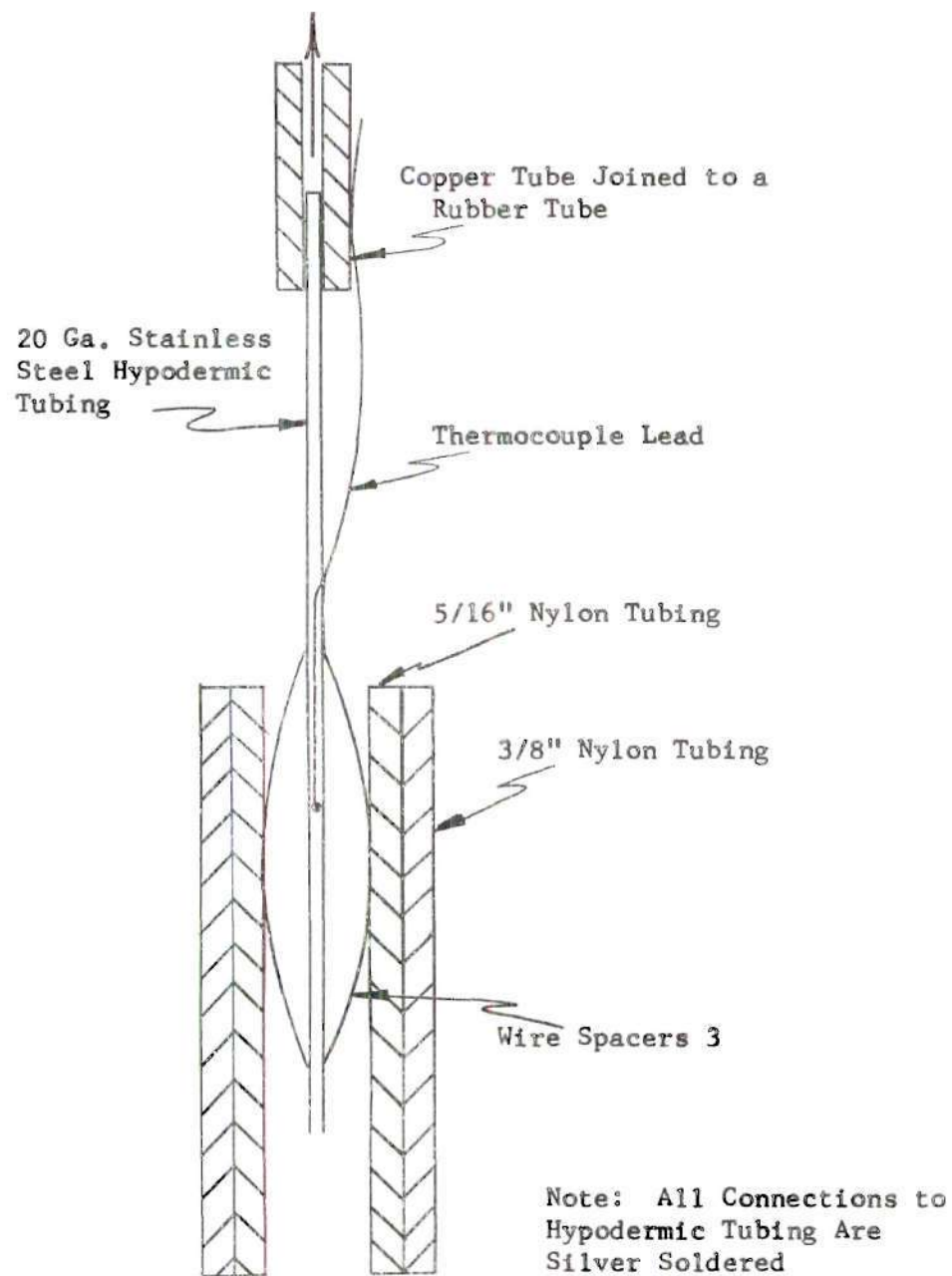




Detail A

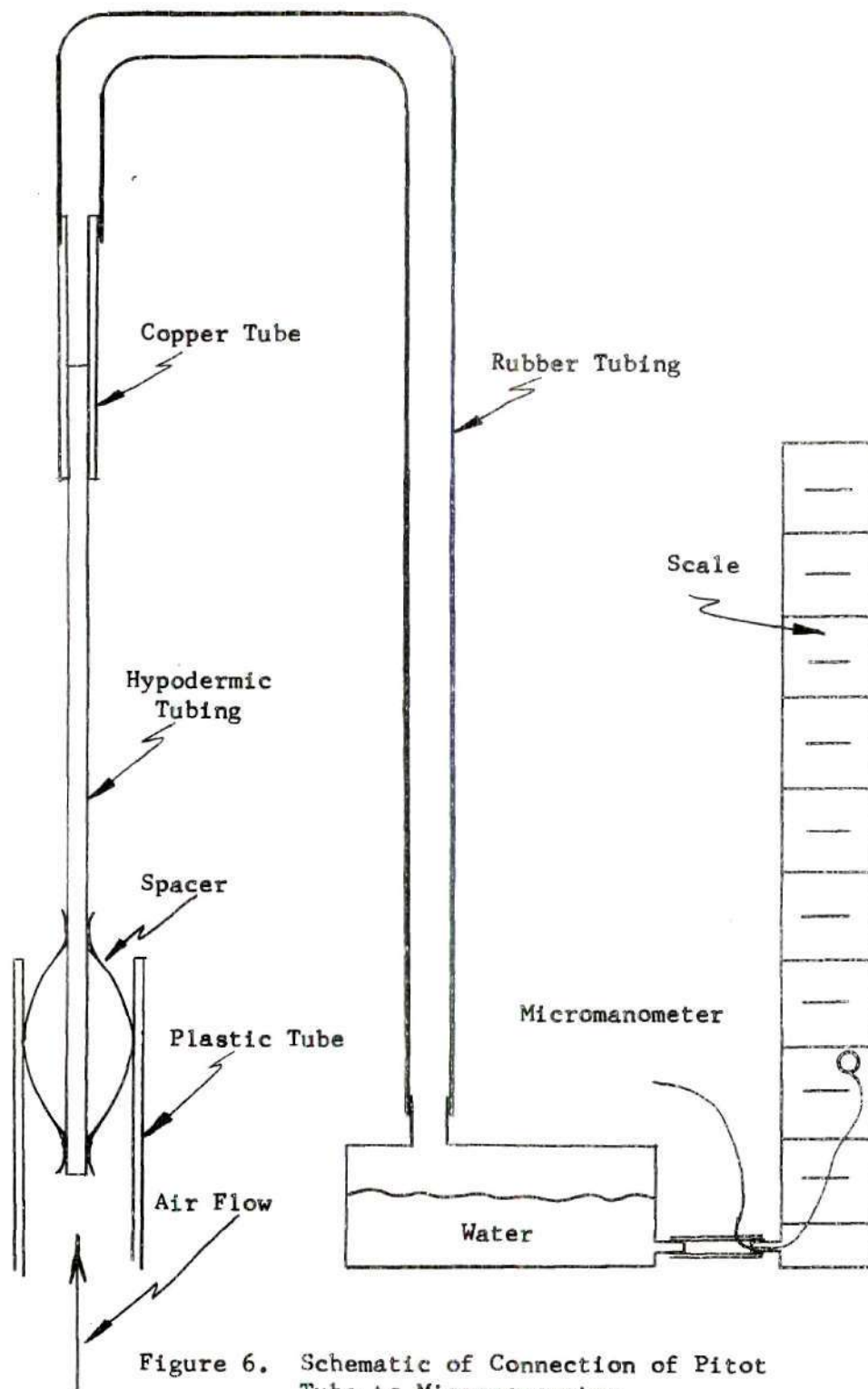
Figure 4. Detail of Manifold Port Construction

## To Manometer Manifold



Detail B

Figure 5. Detail of Pitot Tube



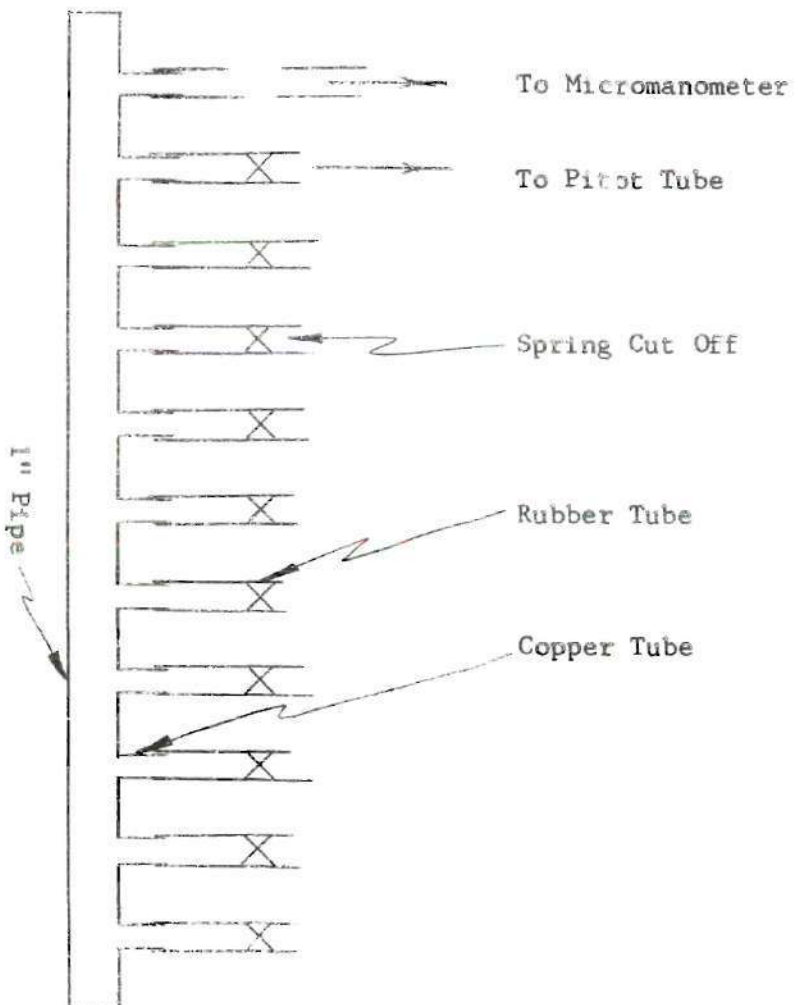


Figure 7. Schematic of Switching Manifold  
for Pitot Tubes

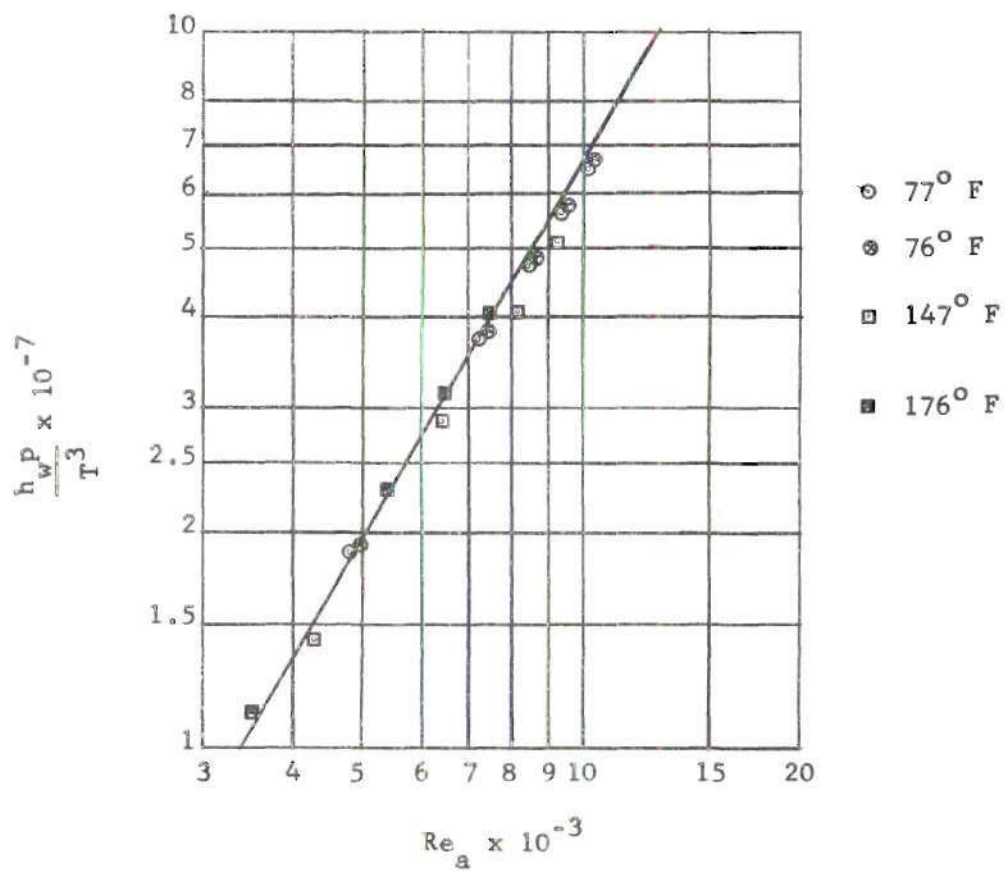


Figure 8. Correlation of Pitot Tubes

$$M_o = 1$$

$$Q_o = 1$$

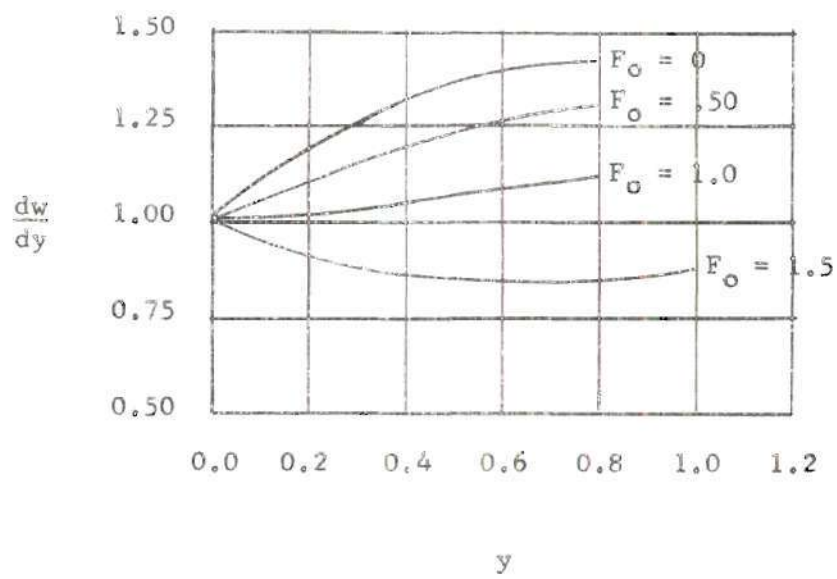


Figure 9. Calculated Side-flow Distributions



$$M_o = 1.0$$

$$Q_o = 0.8$$

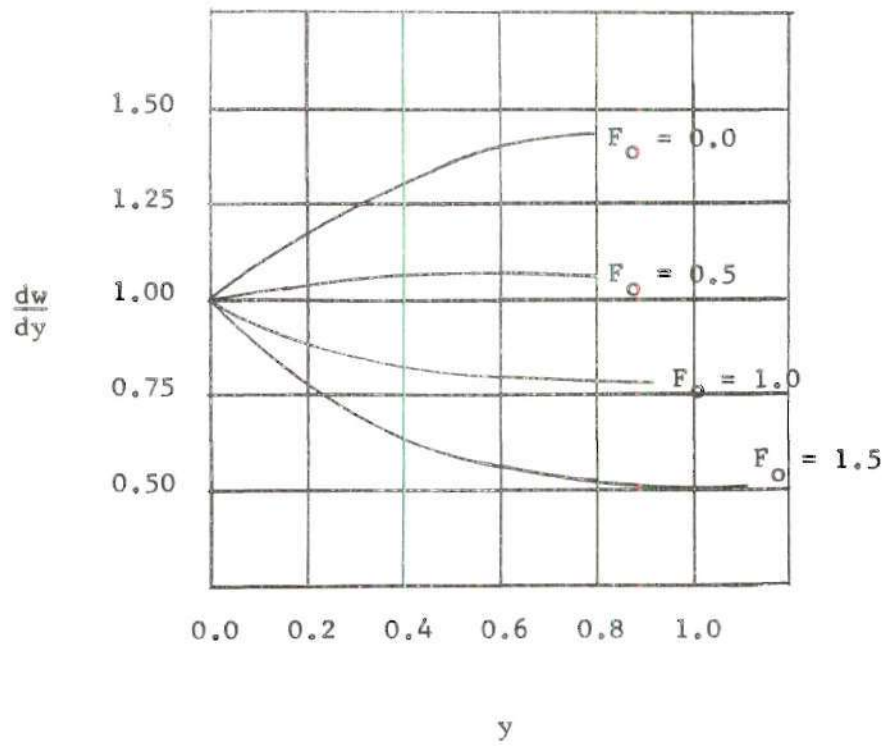


Figure 10. Calculated Side-flow Distributions

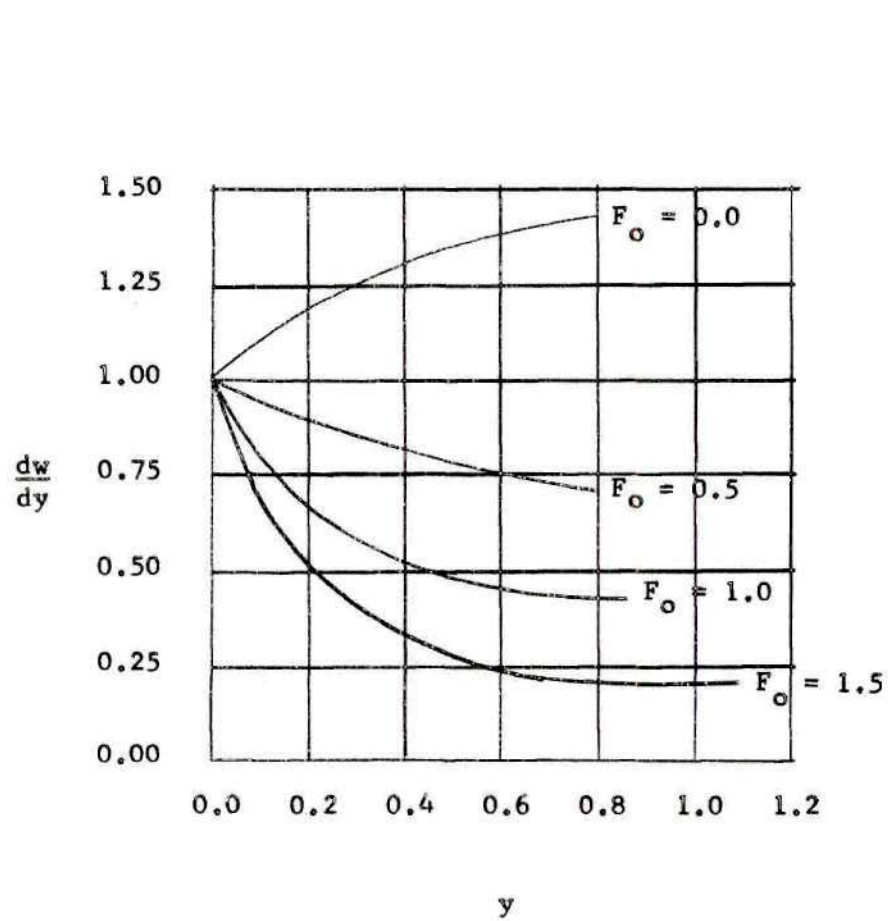


Figure 11. Calculated Side-flow Distributions

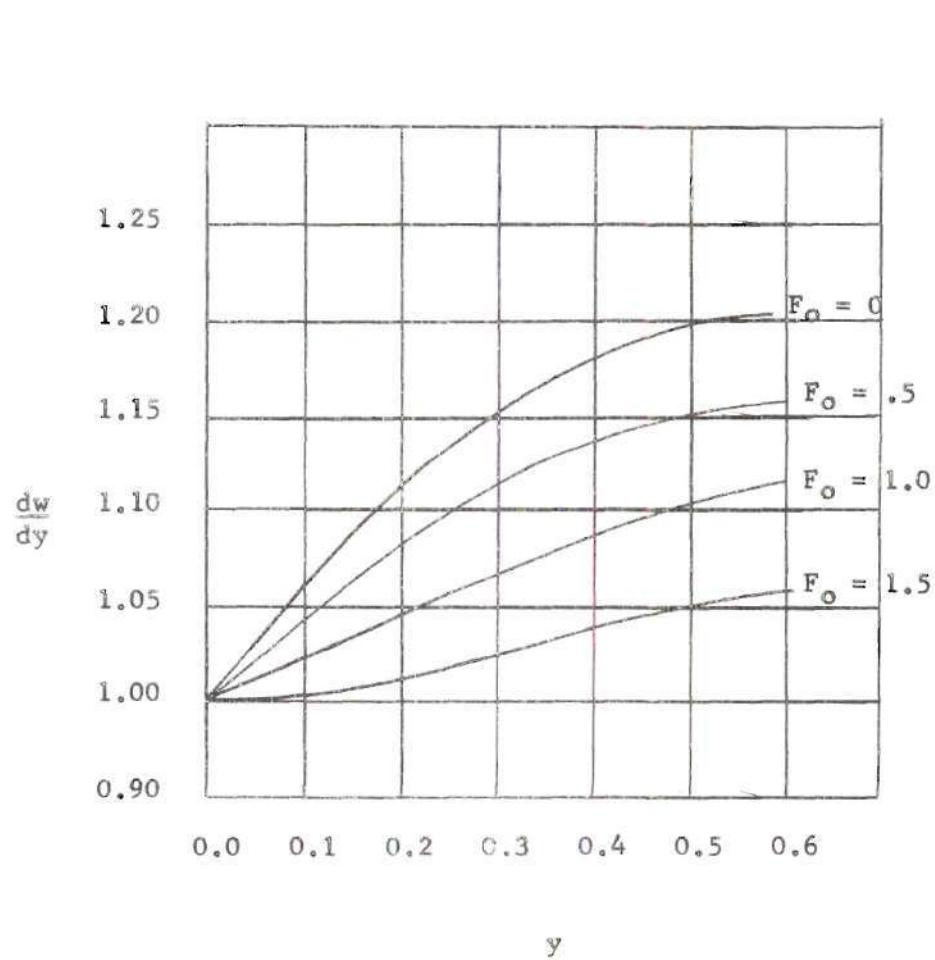


Figure 12. Calculated Side-flow Distributions

$$M_o = 1.5$$

$$\Theta_o = 0.8$$

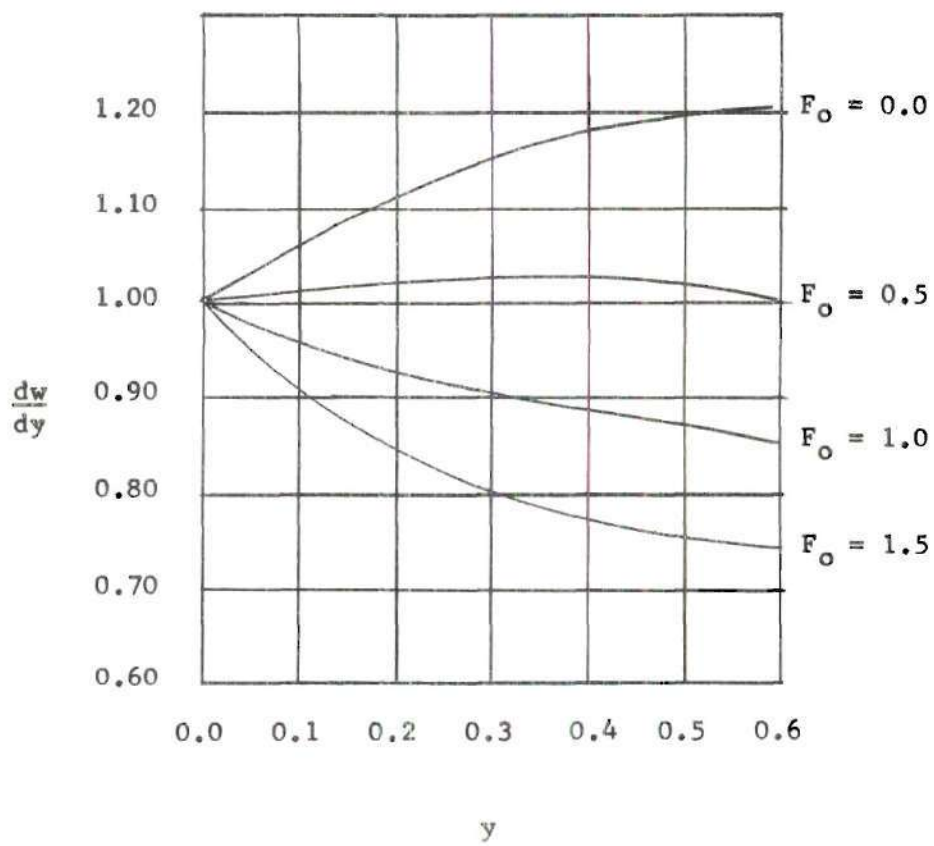


Figure 13. Calculated Side-flow Distributions

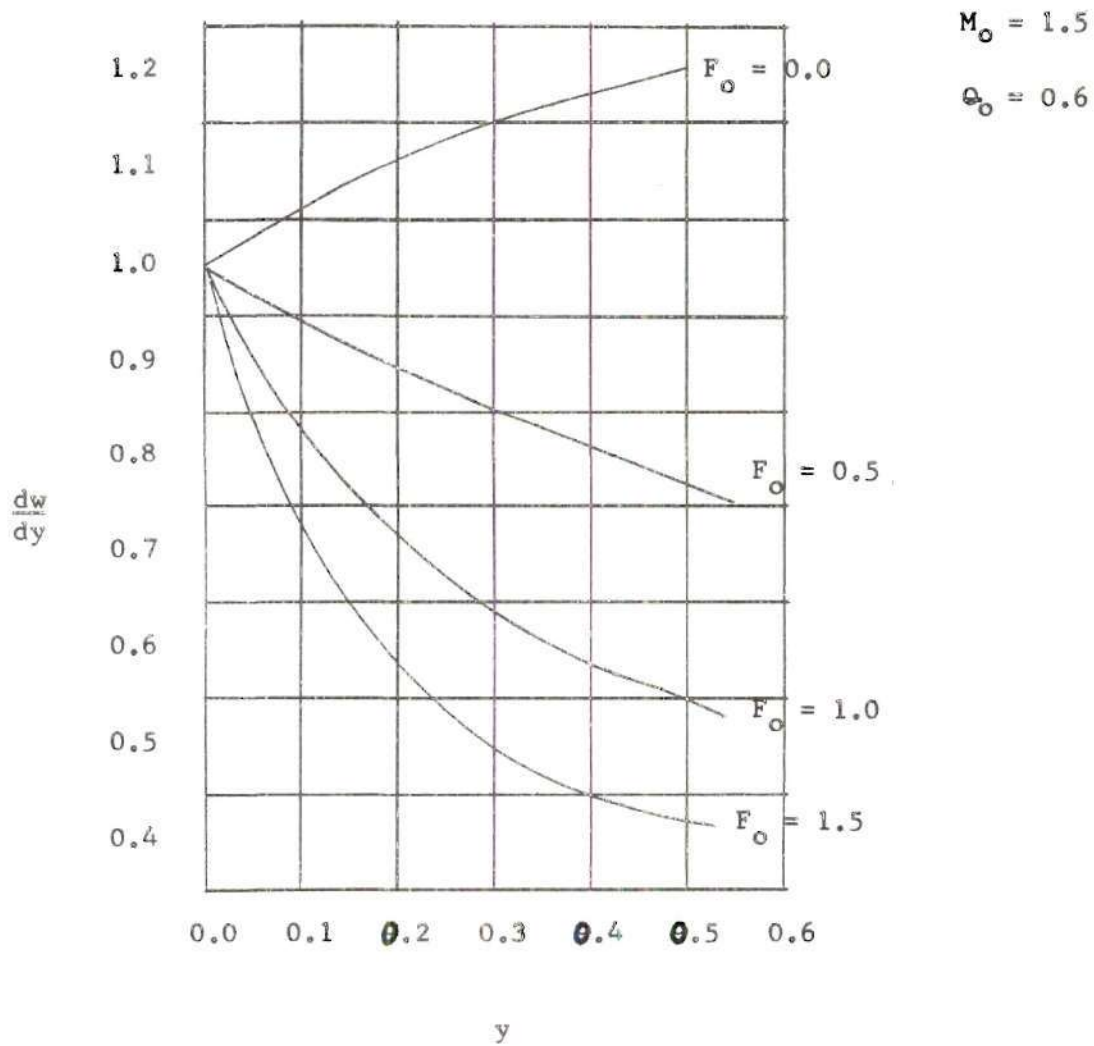


Figure 14. Calculated Side-flow Distributions

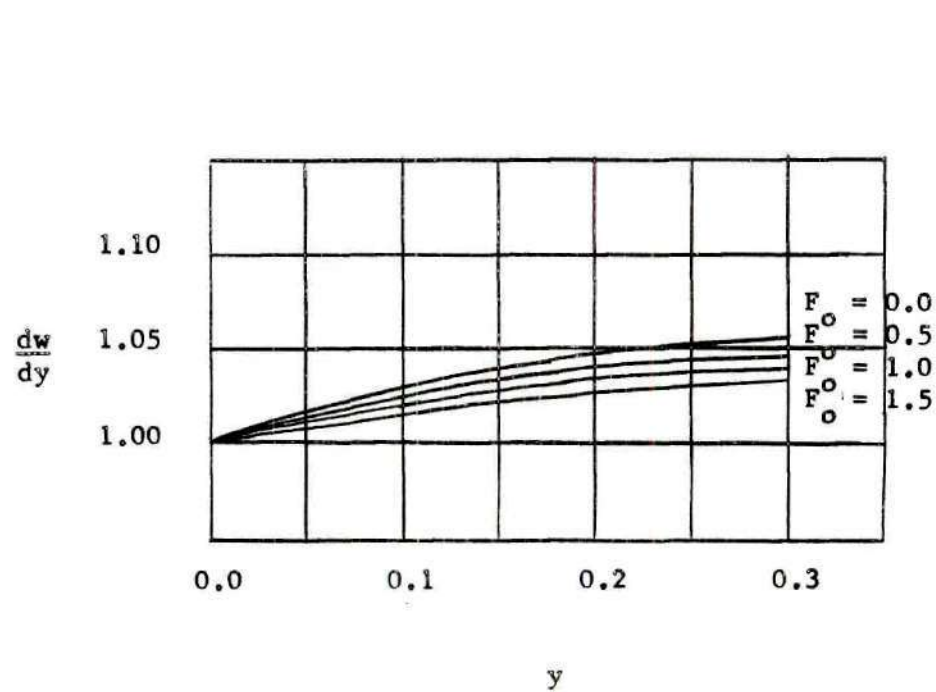


Figure 15. Calculated Side-flow Distributions



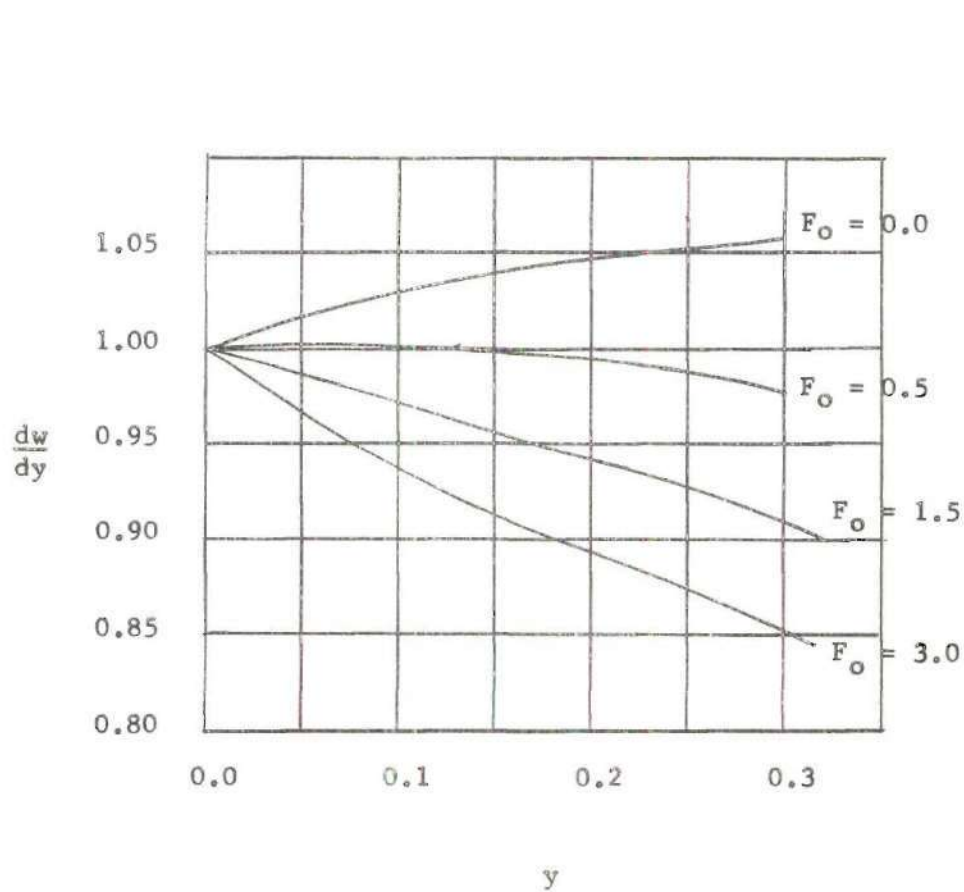


Figure 16. Calculated Side-flow Distributions

$$M_0 = 3.0$$

$$Q_0 = 0.6$$

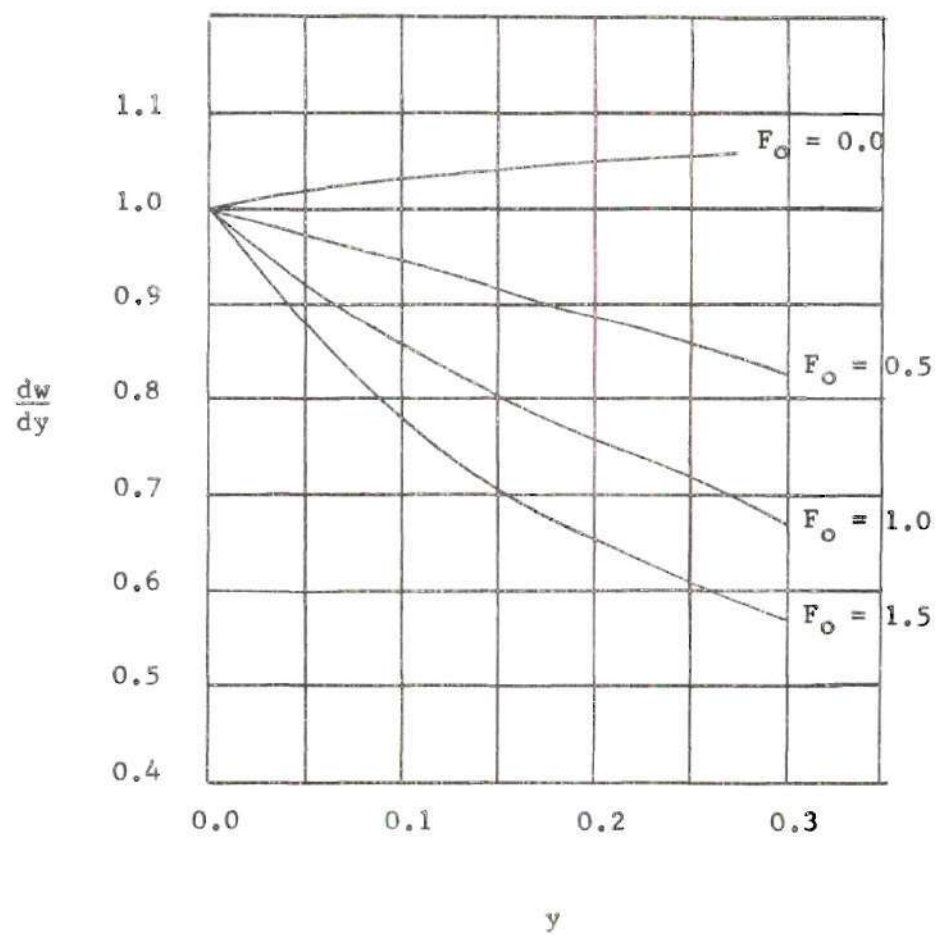


Figure 17. Calculated Side-flow Distributions

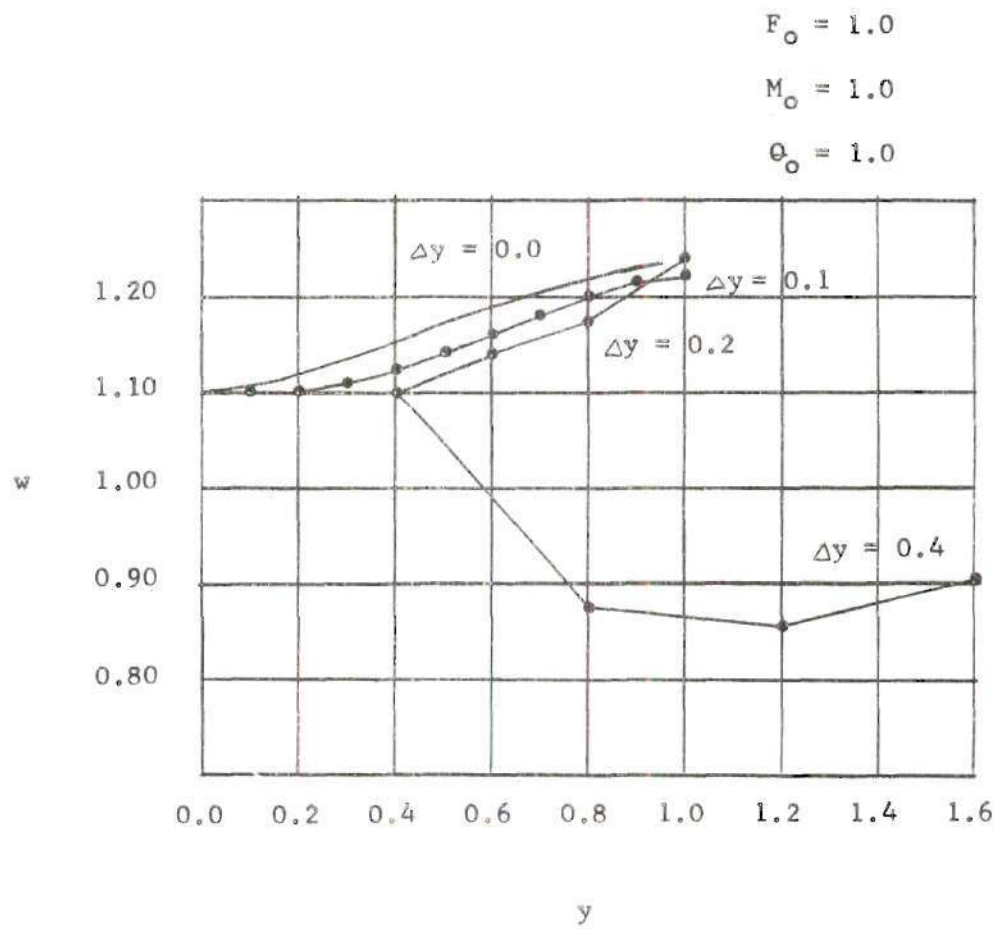


Figure 18. Effects of Finite Distance Between Ports on Flow Distribution

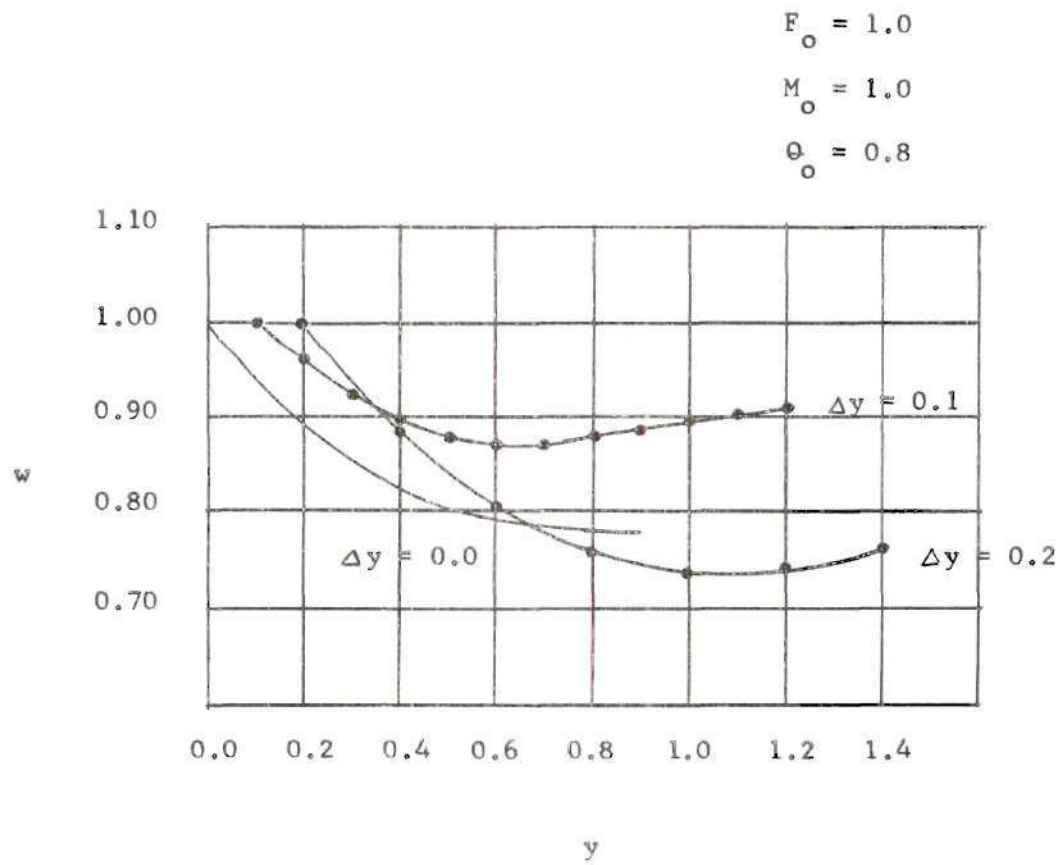


Figure 19. Effects of Finite Distance Between Ports on Flow Distribution

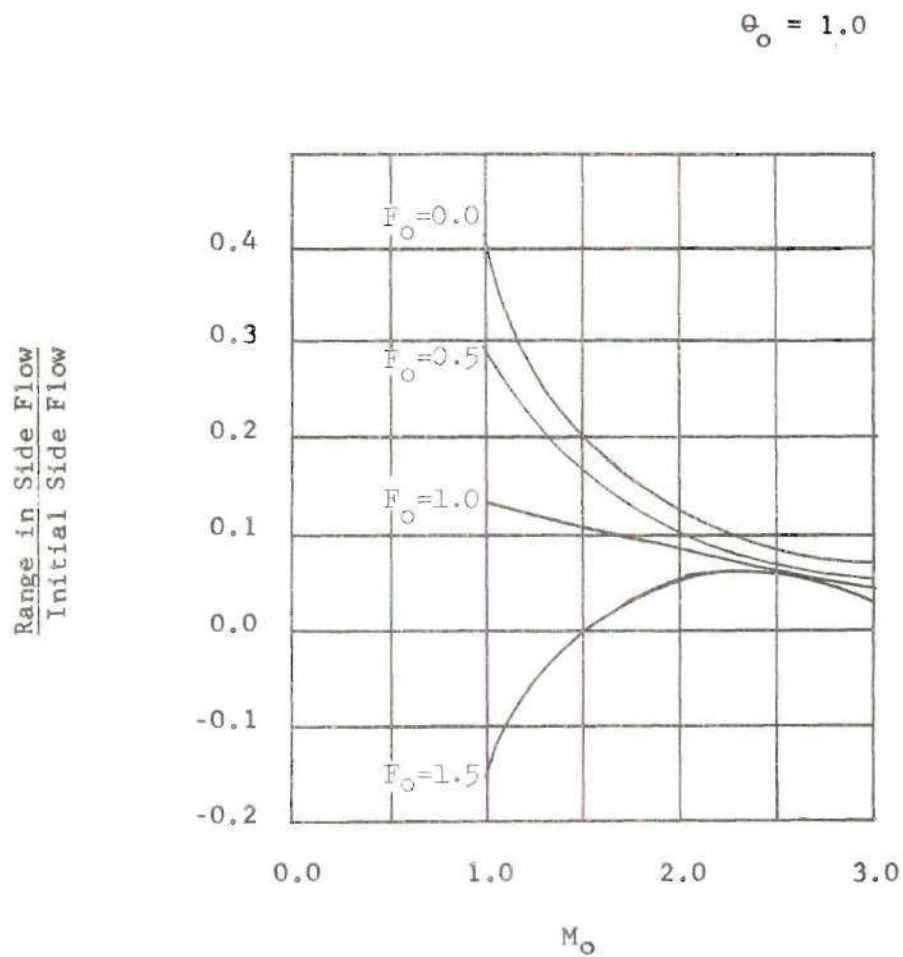


Figure 20. Difference of Extreme Values of Calculated Side Flow

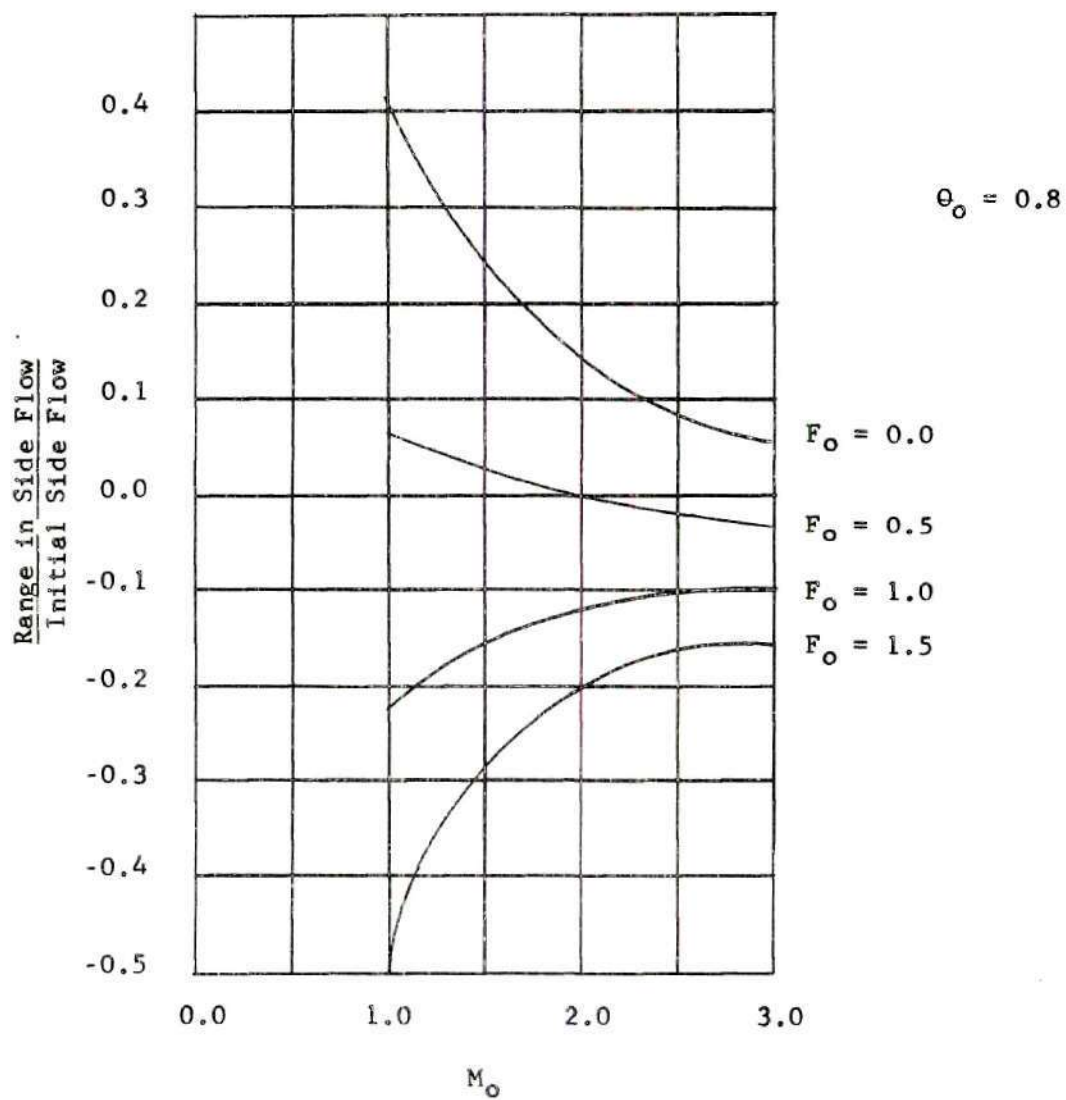


Figure 21. Difference of Extreme Values  
of Calculated Side Flow

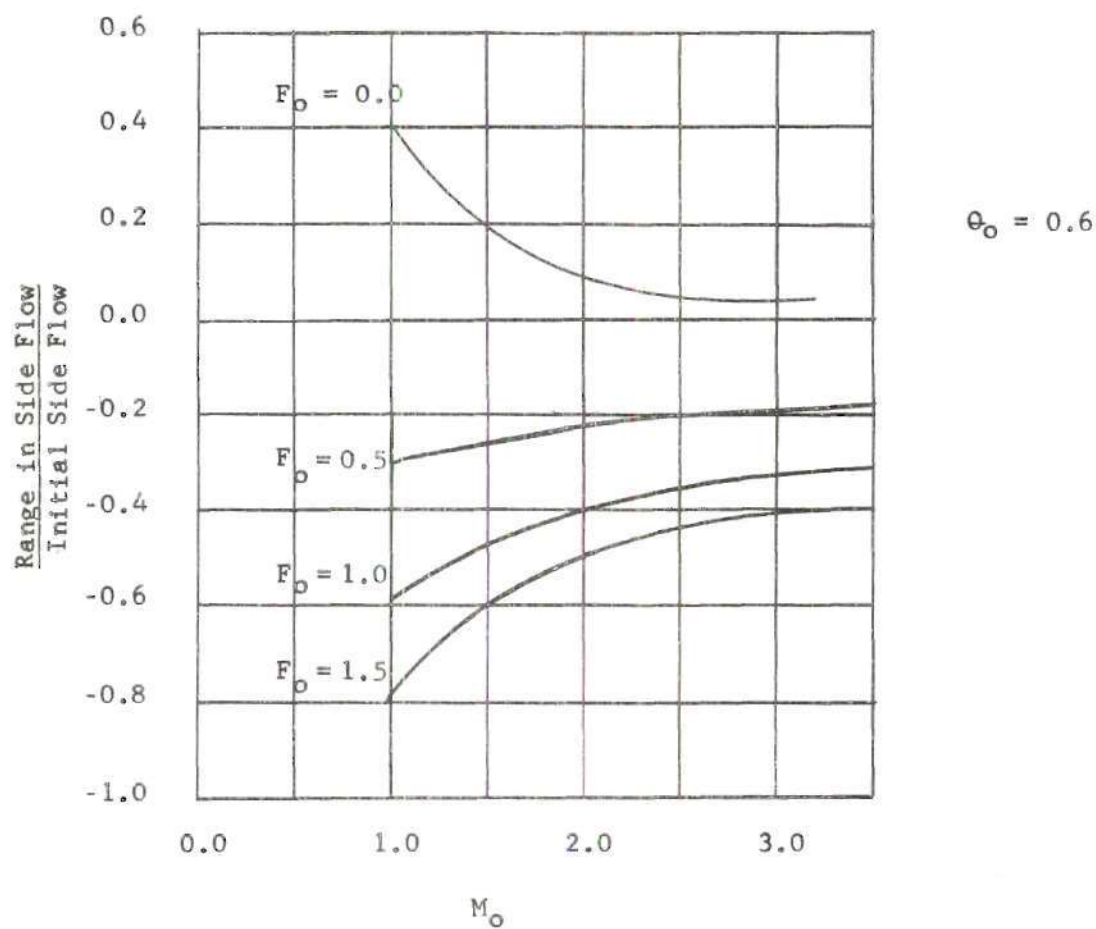


Figure 22. Difference of Extreme Values of Calculated Side Flow



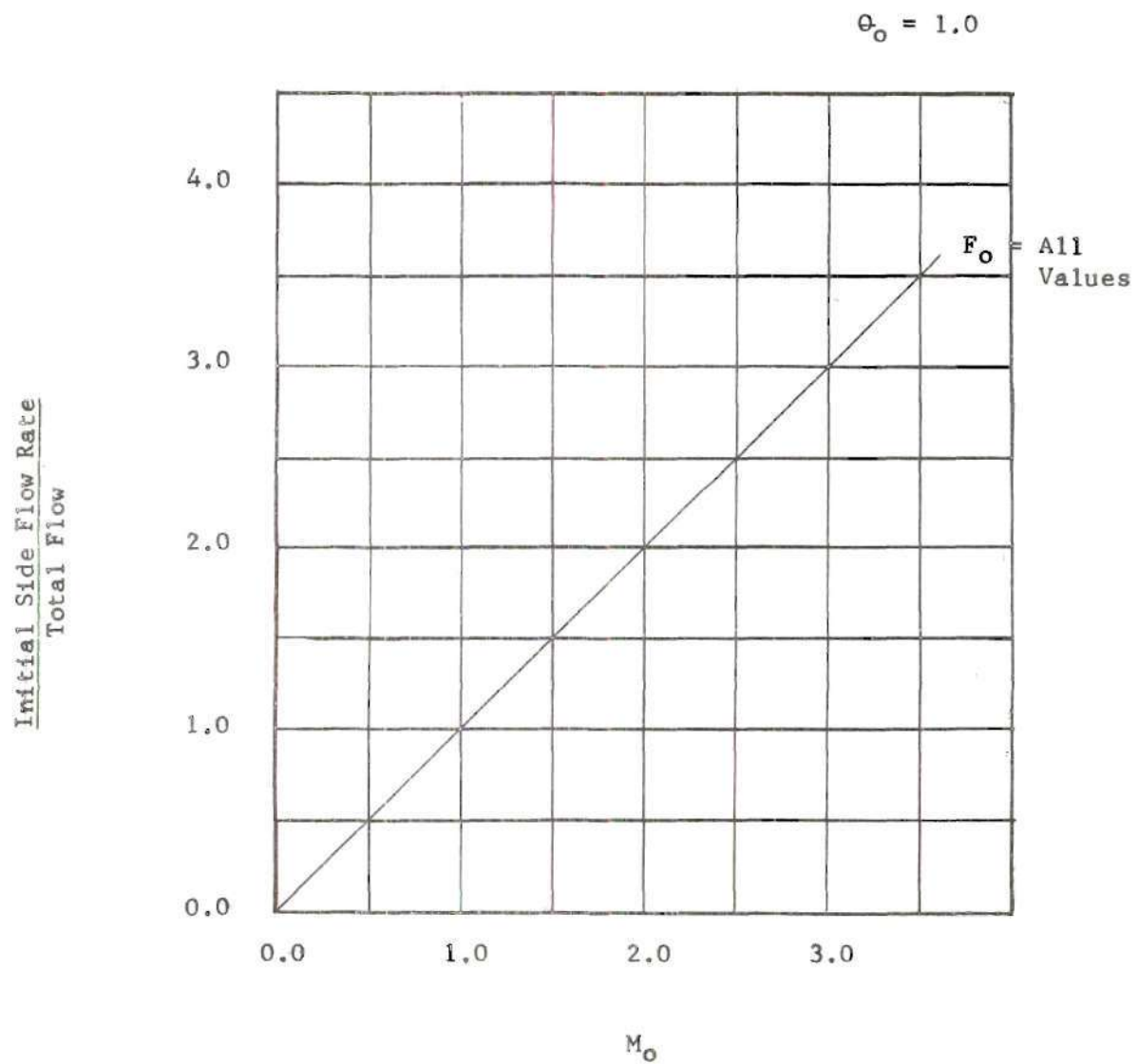


Figure 23. Initial Side Flow Rate for Calculated Side Flow

$$\theta_o = 0.8$$

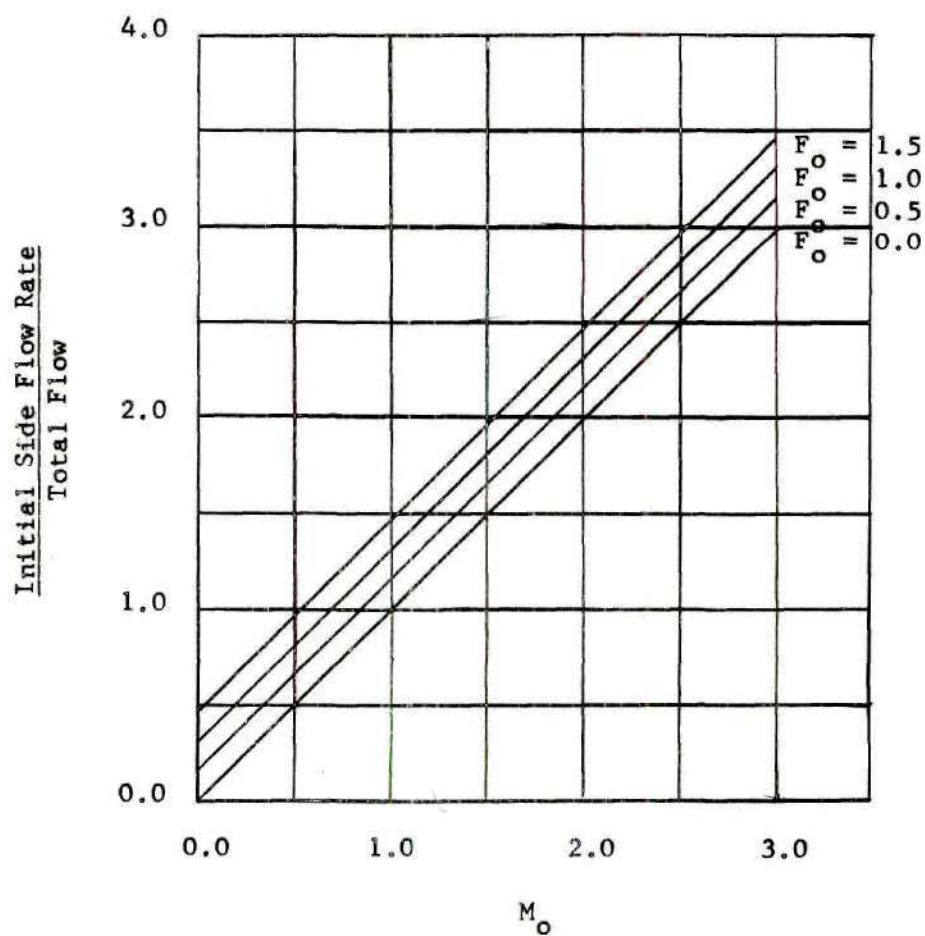


Figure 24. Initial Side Flow Rate for Calculated Side Flow

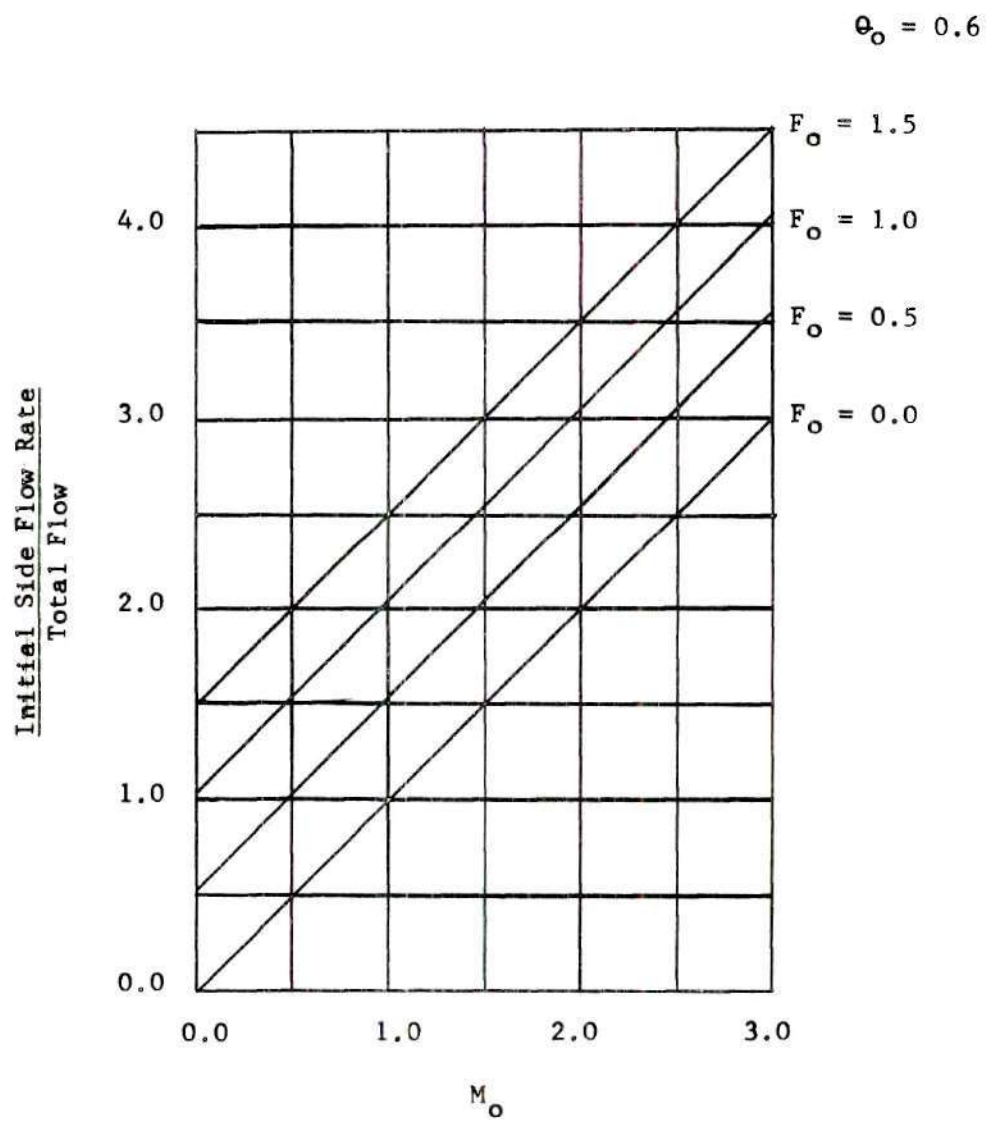
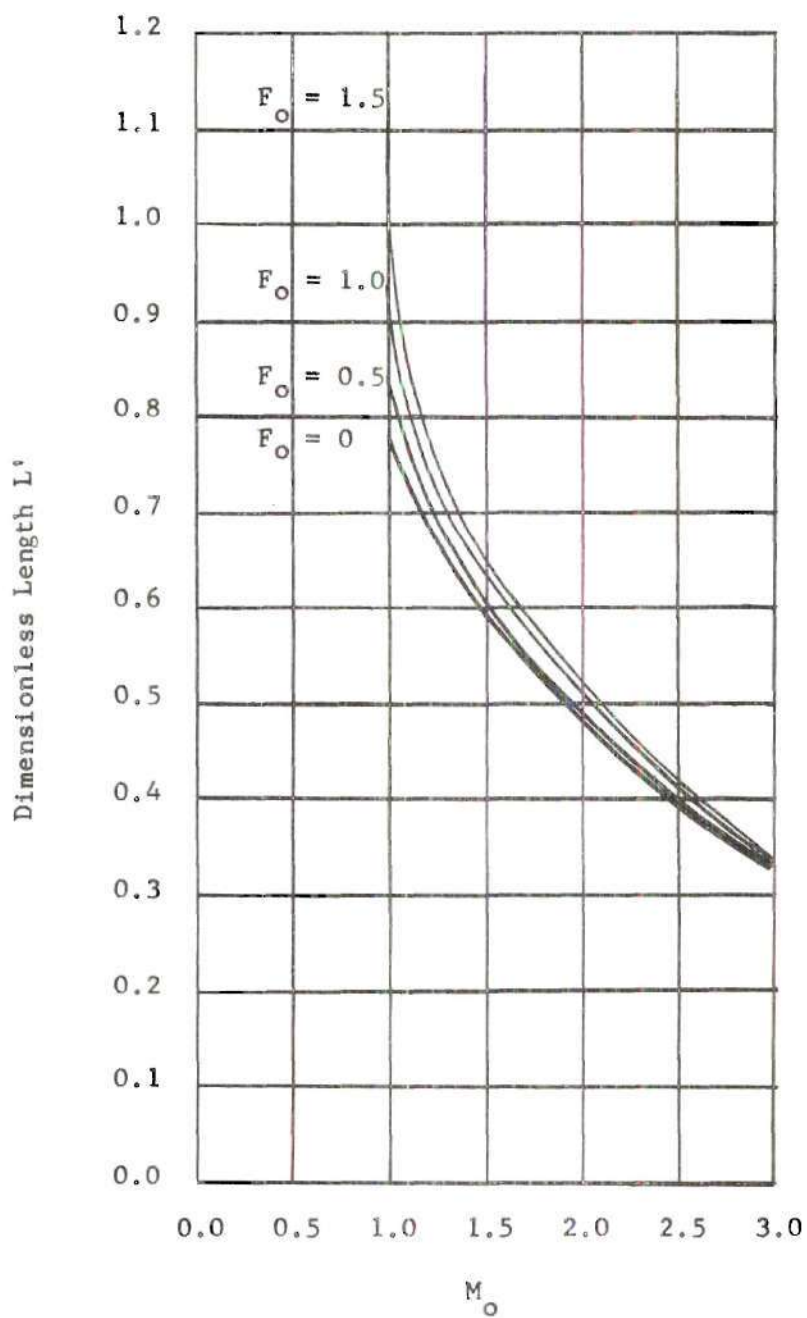


Figure 25. Initial Side Flow Rate for Calculated Side Flow



$$\theta_O = 1.0$$

Figure 26. Dimensionless Length Required to Discharge Total Input Stream

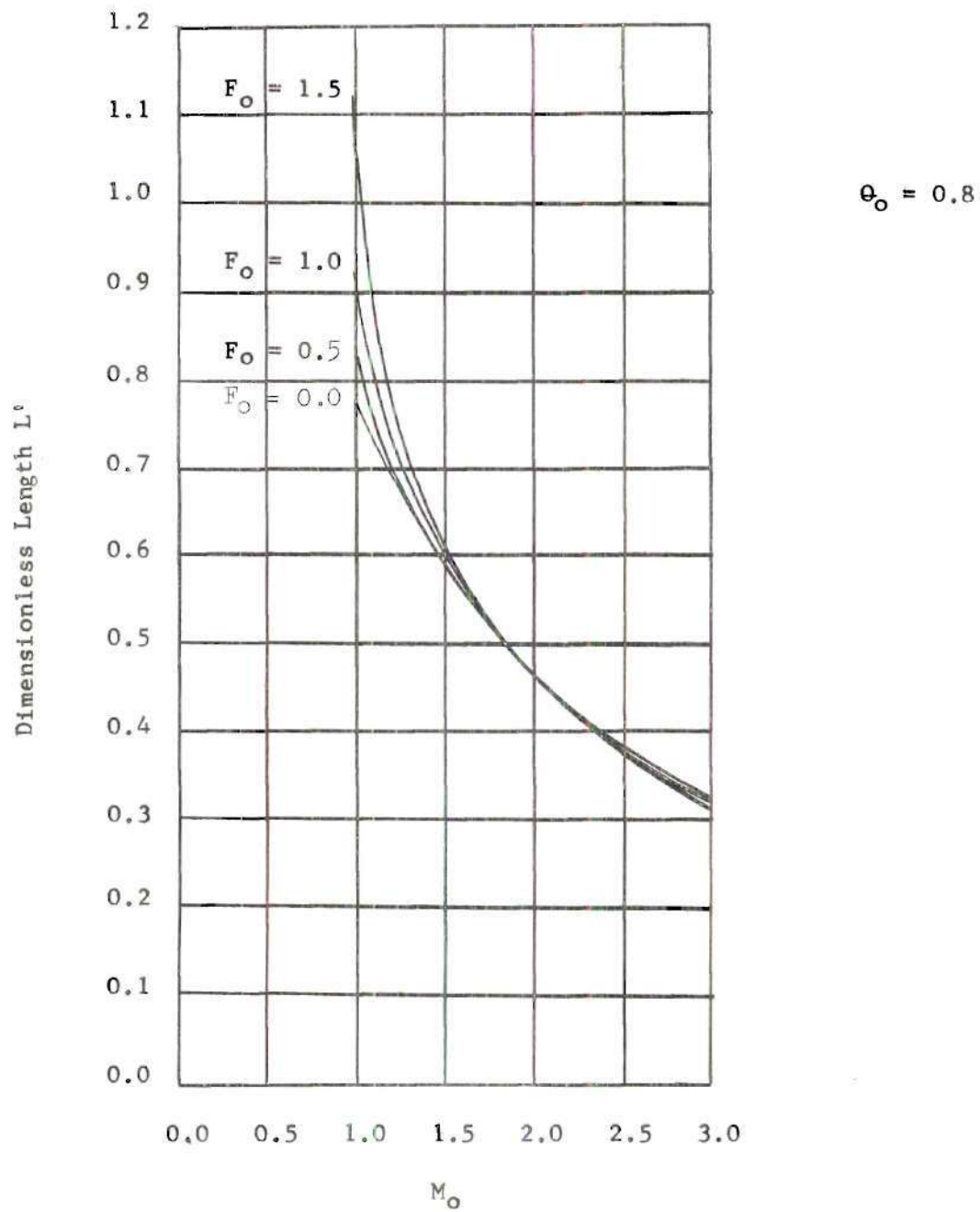


Figure 27. Dimensionless Length Required to Discharge Total Input Stream

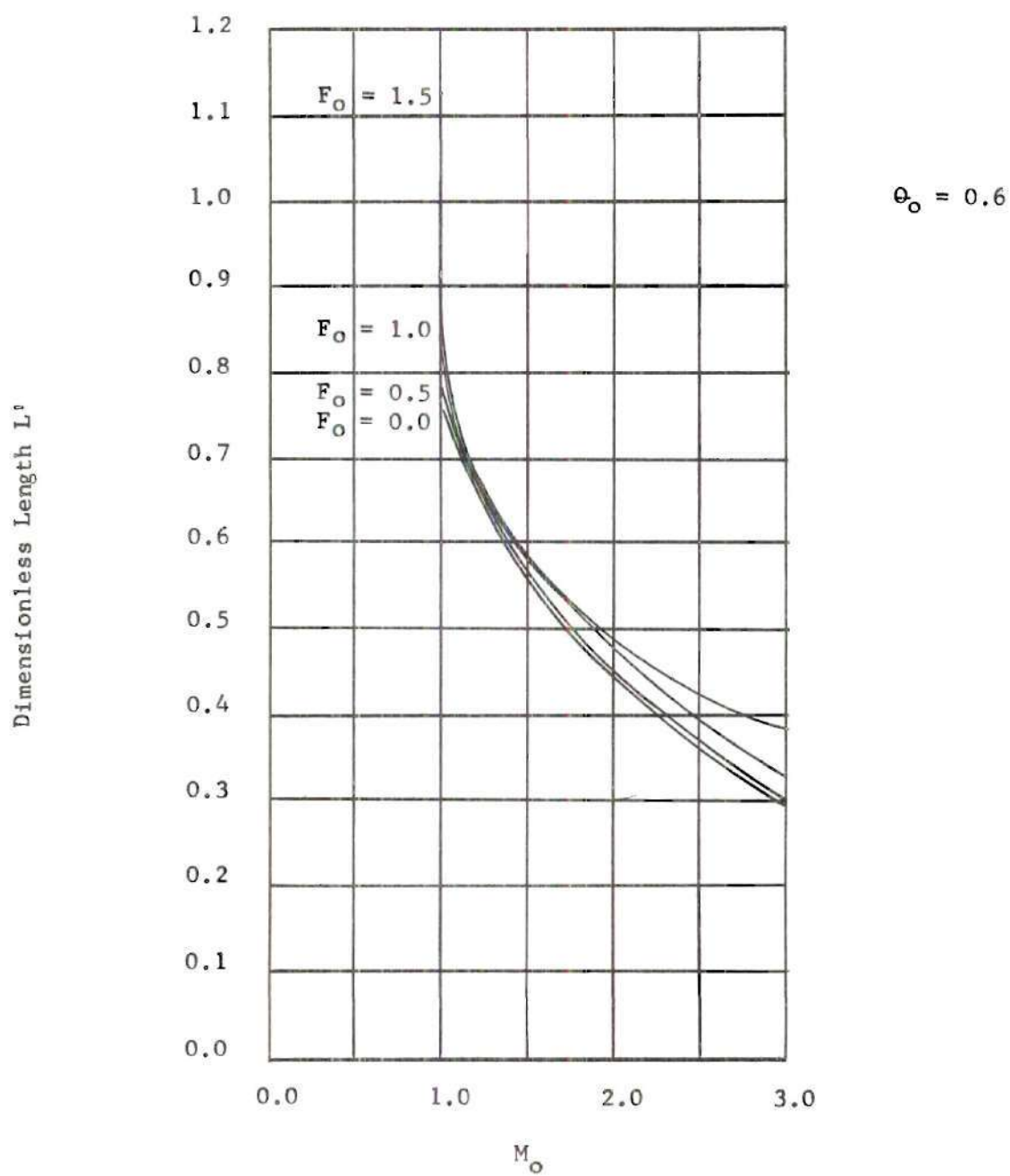


Figure 28. Dimensionless Length Required to Discharge Total Input Stream

Run No. 1

$$F_o = 1.097$$

$$\Theta_o = 1.0$$

$$M_o = 1.854$$

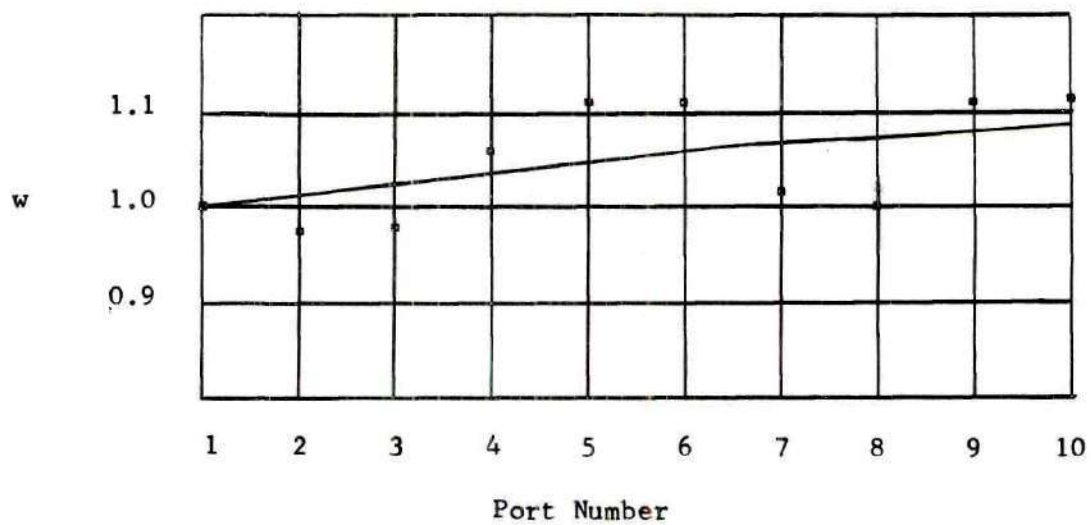


Figure 29. Experimental Side Flow Distributions



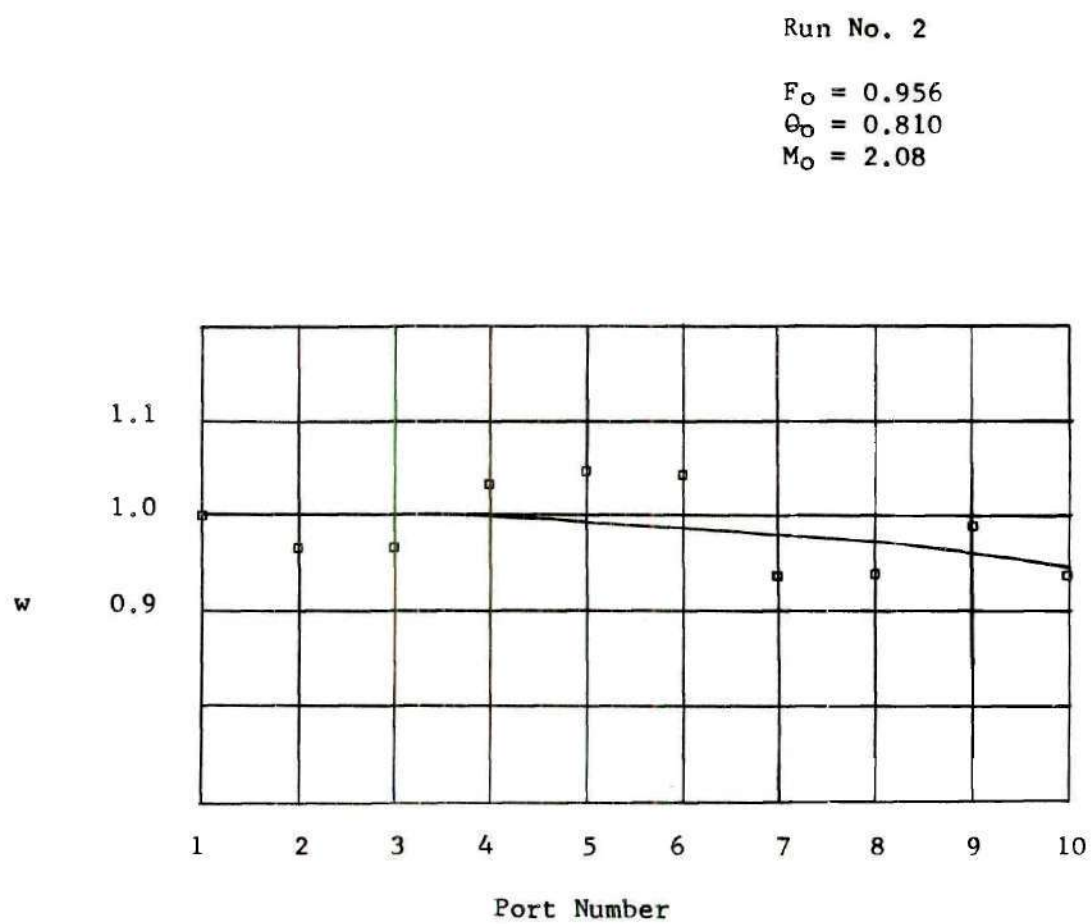


Figure 30. Experimental Side Flow Distributions

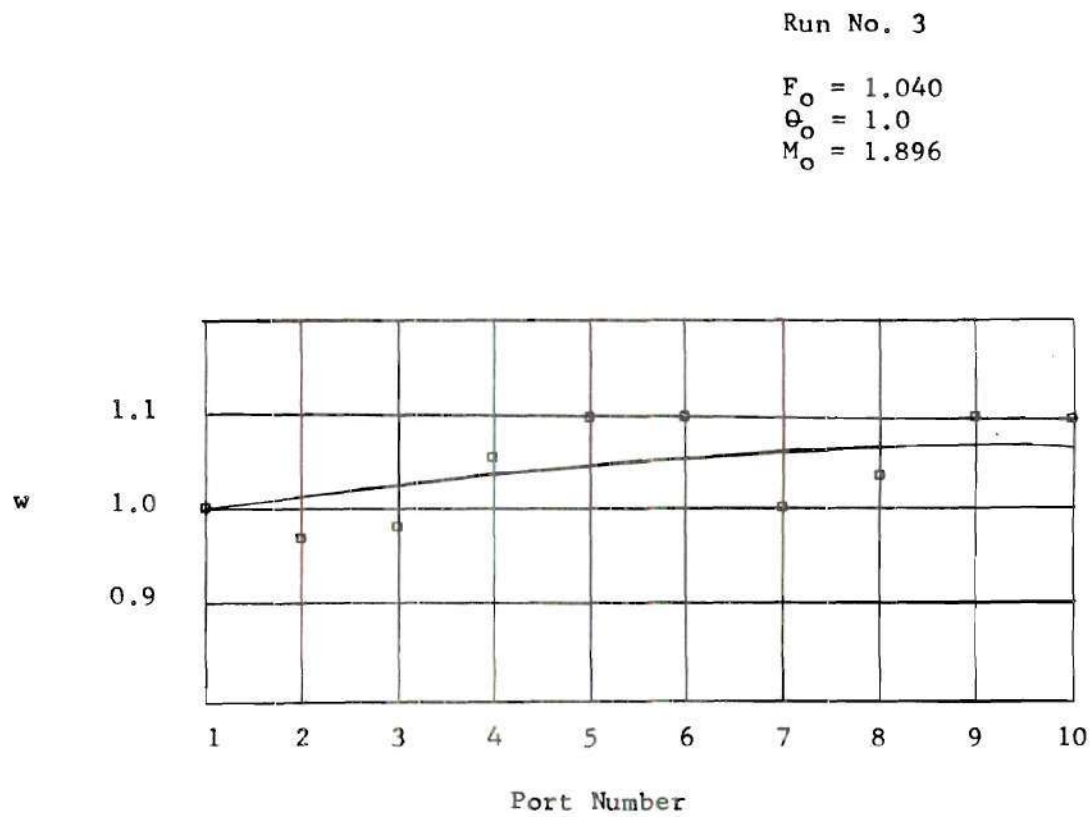


Figure 31. Experimental Side Flow Distributions

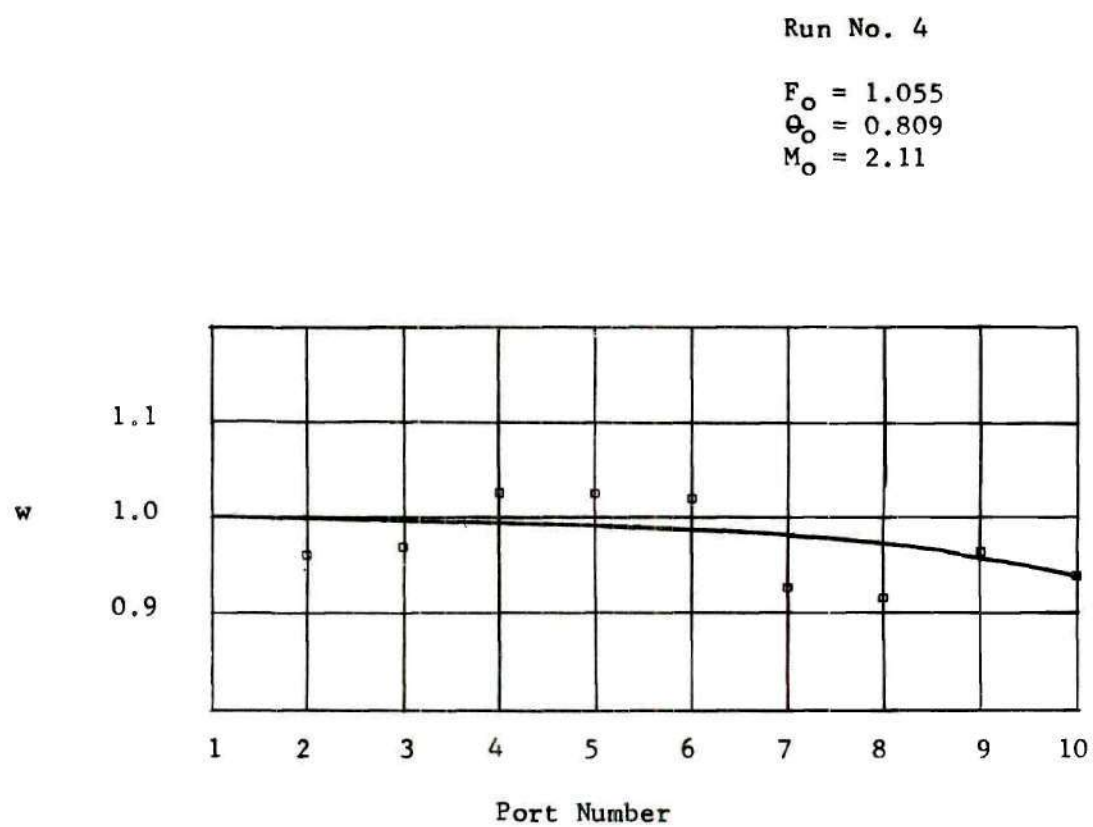


Figure 32. Experimental Side Flow Distributions

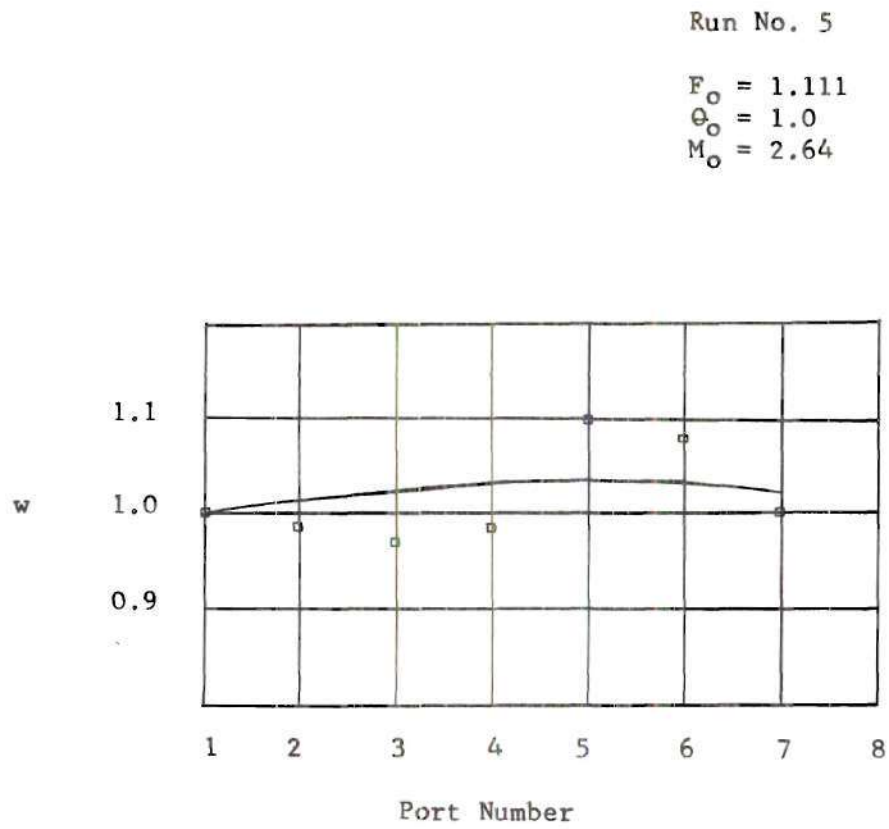


Figure 33. Experimental Side Flow Distributions

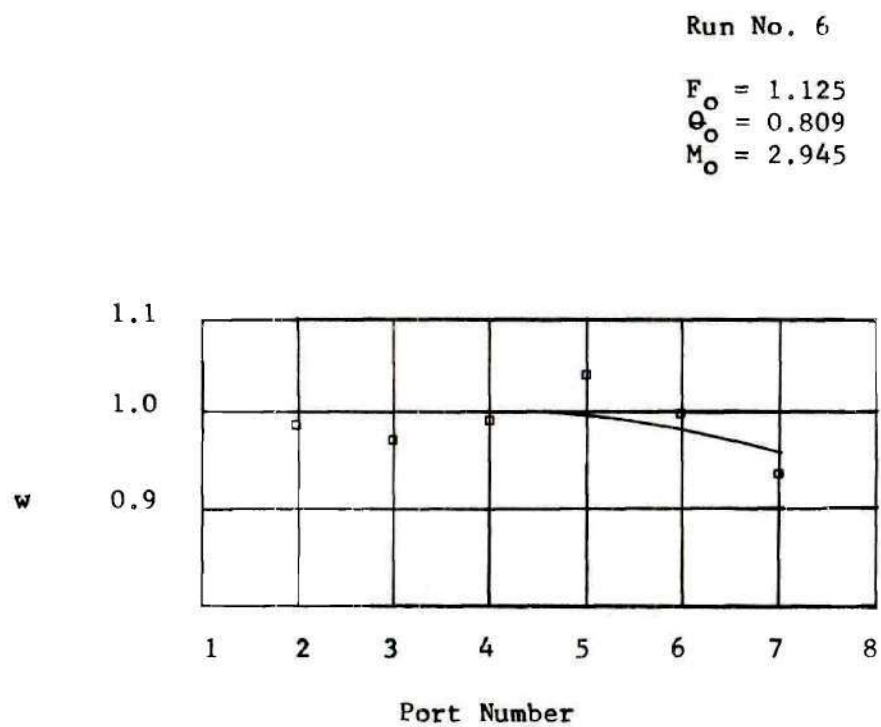


Figure 34. Experimental Side Flow Distributions

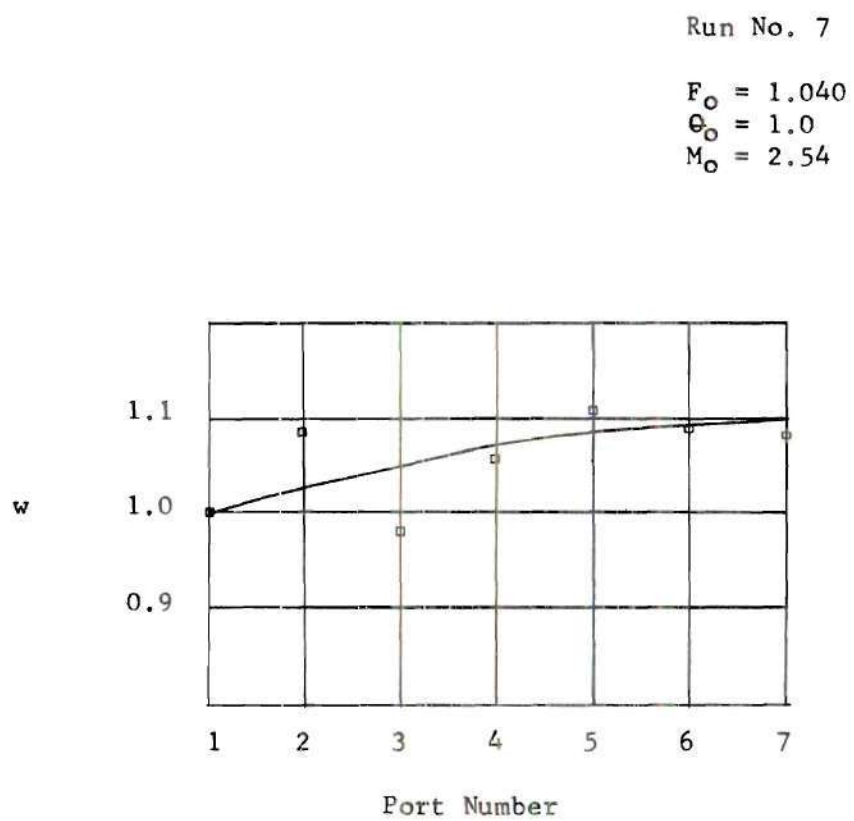


Figure 35. Experimental Side Flow Distributions

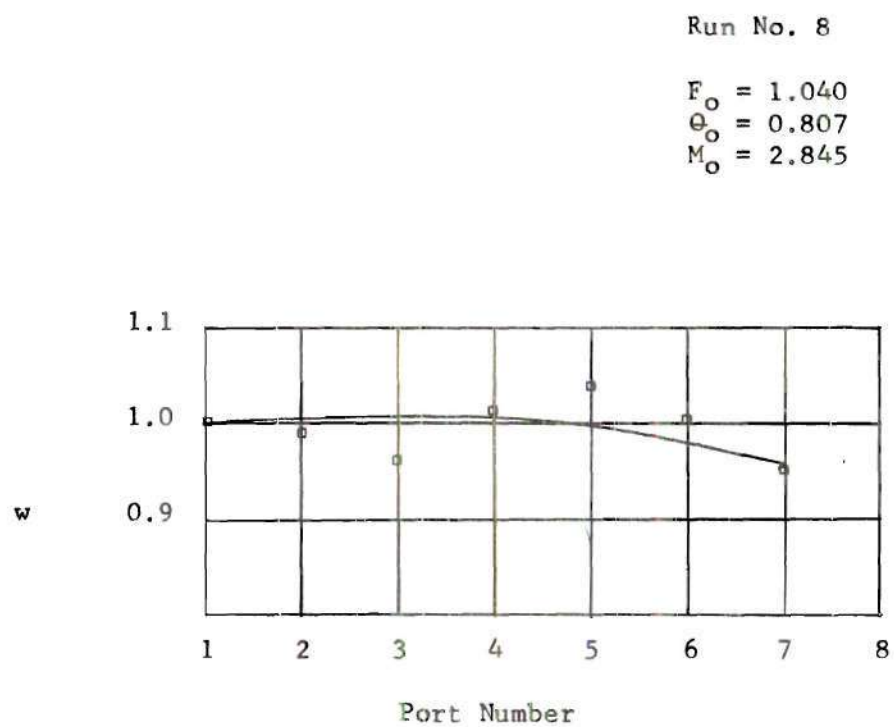


Figure 36. Experimental Side Flow Distributions



Run No. 9

$$F_o = 2.203$$

$$Q_o = 1.0$$

$$M_o = 3.58$$

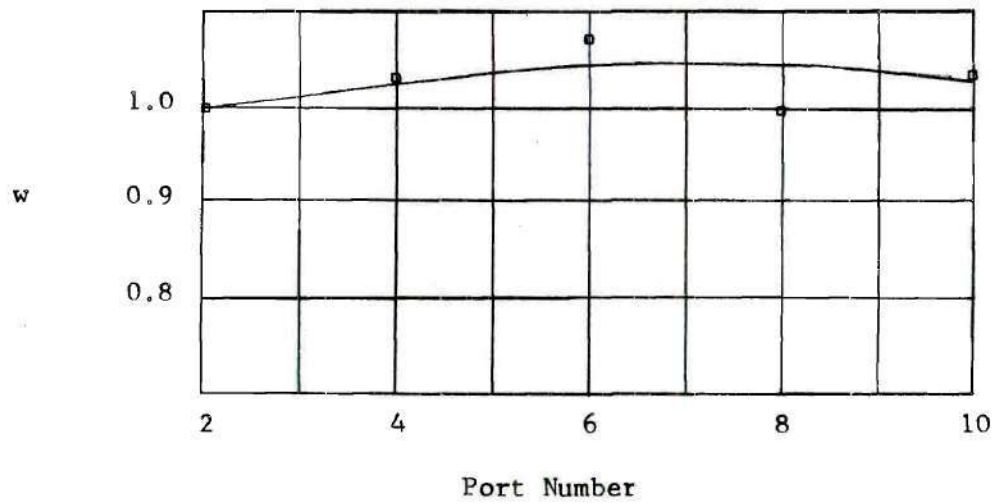


Figure 37. Experimental Side Flow Distributions

Run No. 10

$$F_o = 2.232$$

$$Q_o = 0.817$$

$$M_o = 3.95$$

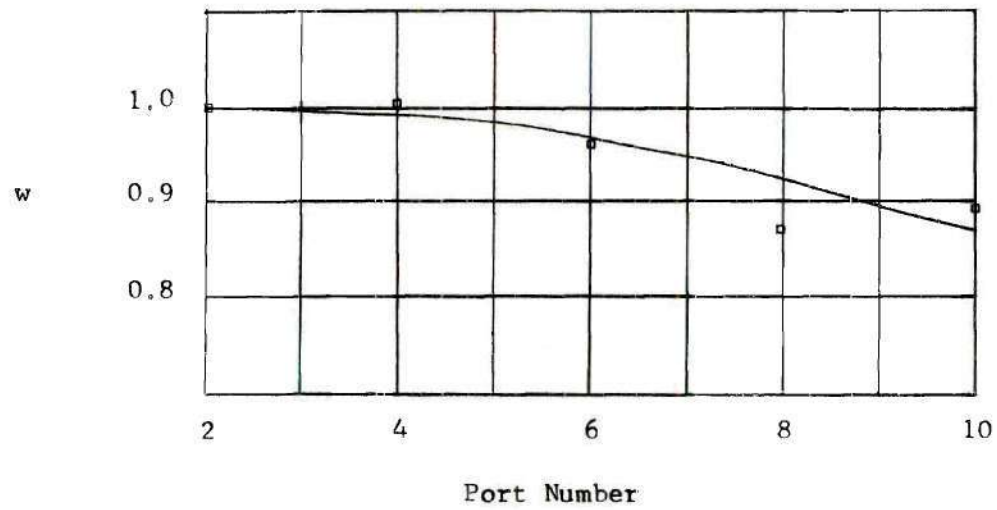


Figure 38. Experimental Side Flow Distributions

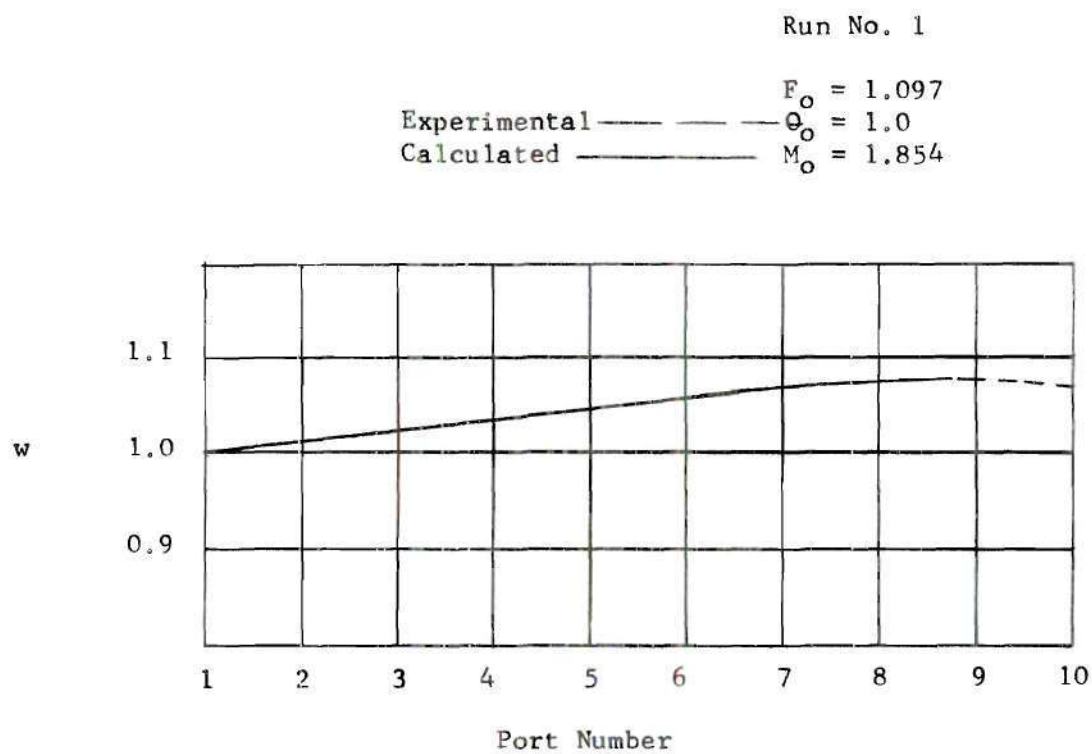


Figure 39. Comparison Between Experimental and Calculated Side Flow Distribution

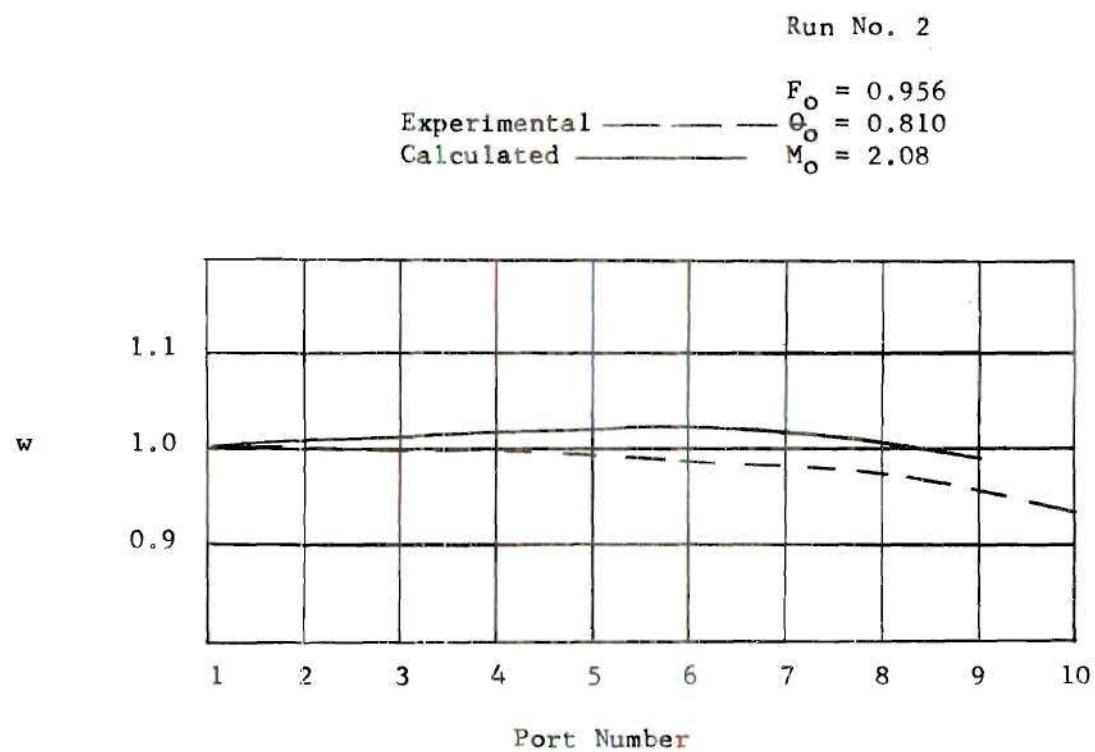


Figure 40. Comparison Between Experimental and Calculated Side Flow Distributions

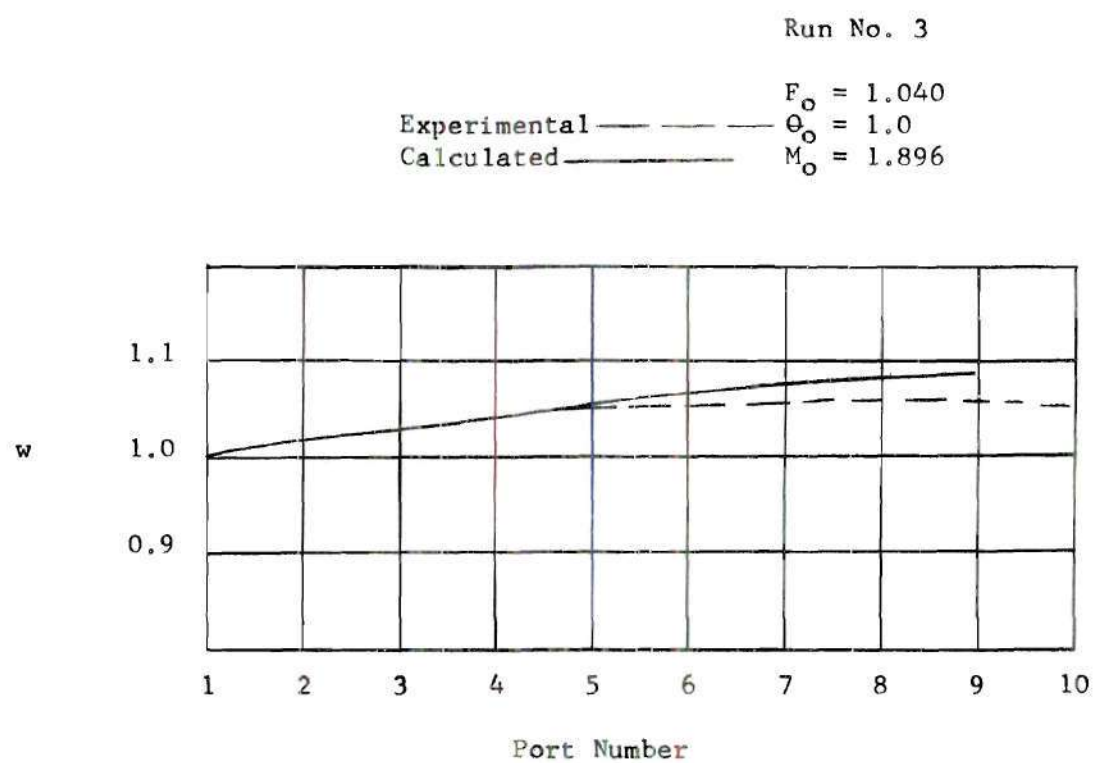


Figure 41. Comparison Between Experimental and Calculated Side Flow Distributions

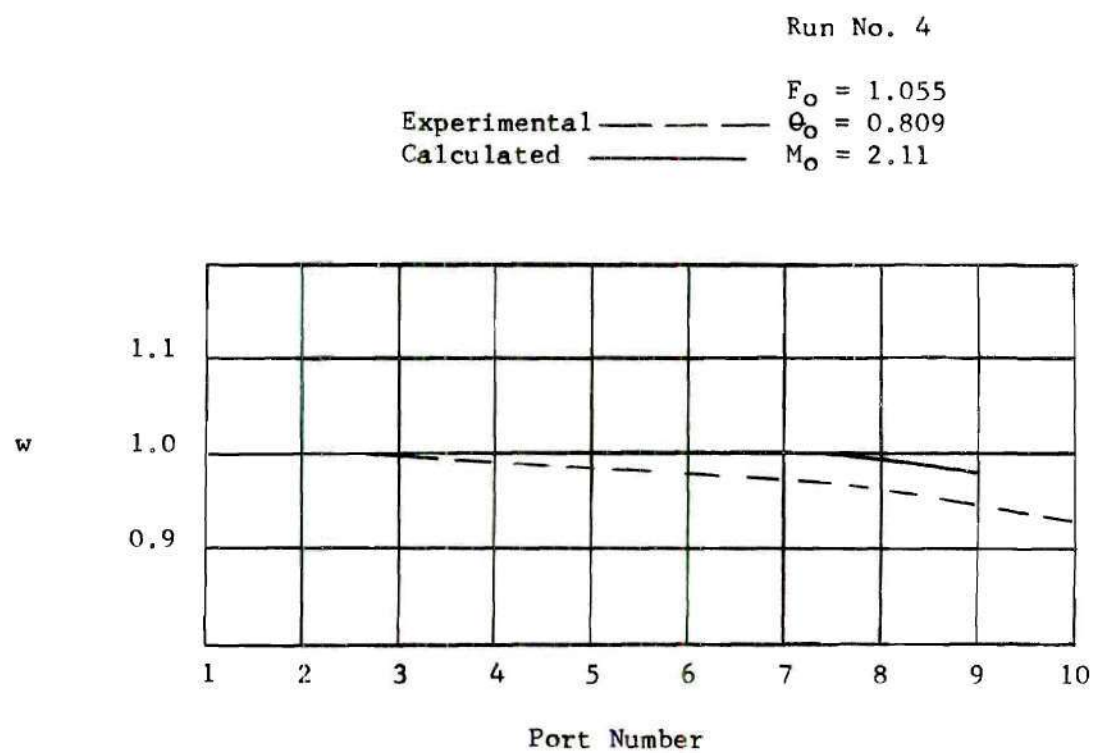


Figure 42. Comparison Between Experimental and Calculated Side Flow Distributions

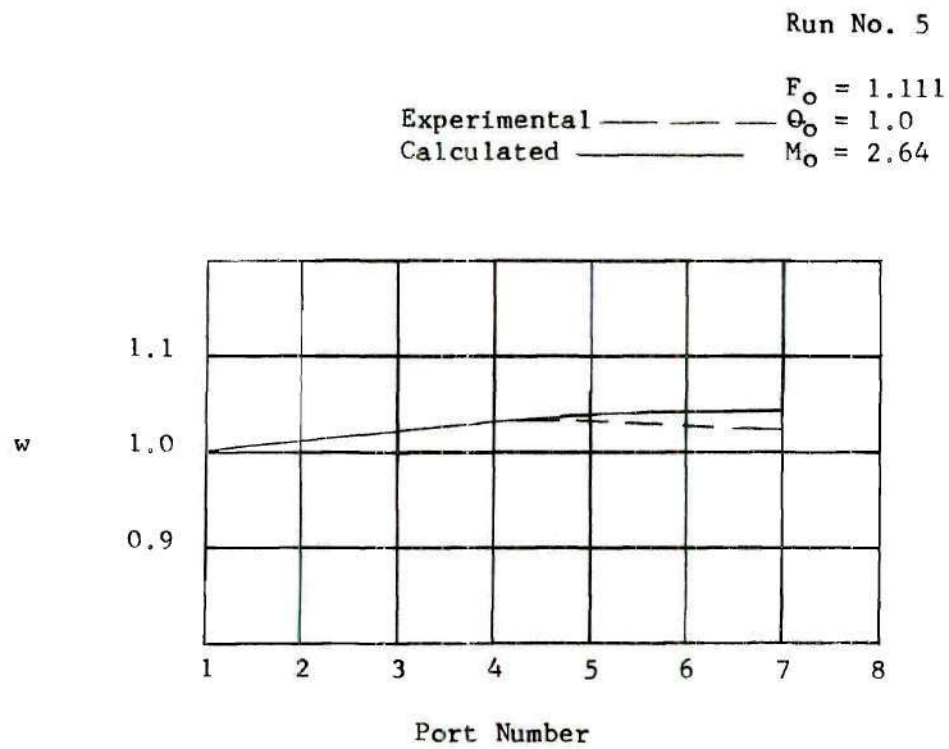


Figure 43. Comparison Between Experimental and Calculated Side Flow Distributions



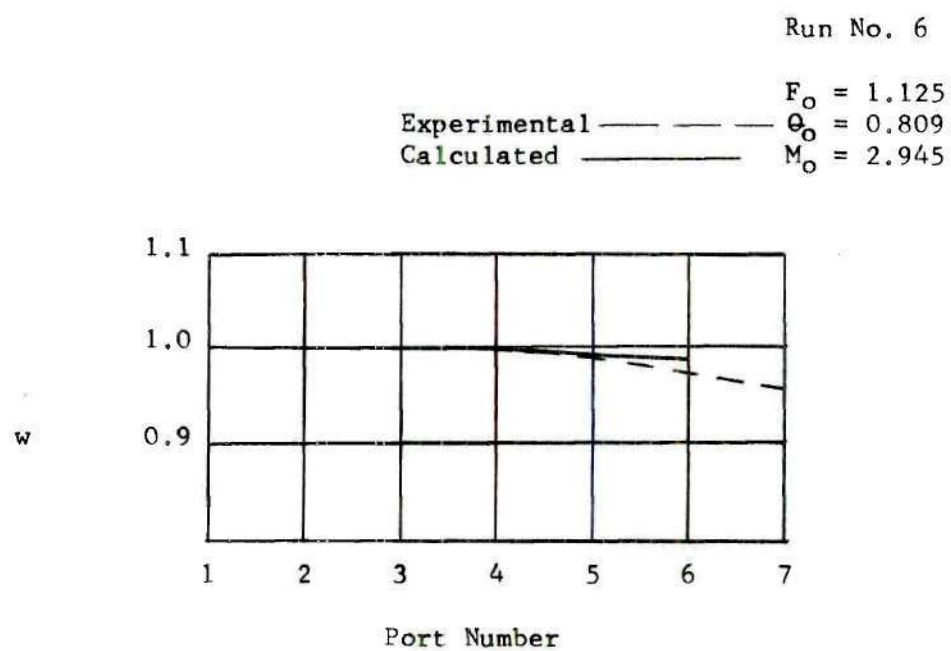


Figure 44. Comparison Between Experimental and Calculated Side Flow Distribution

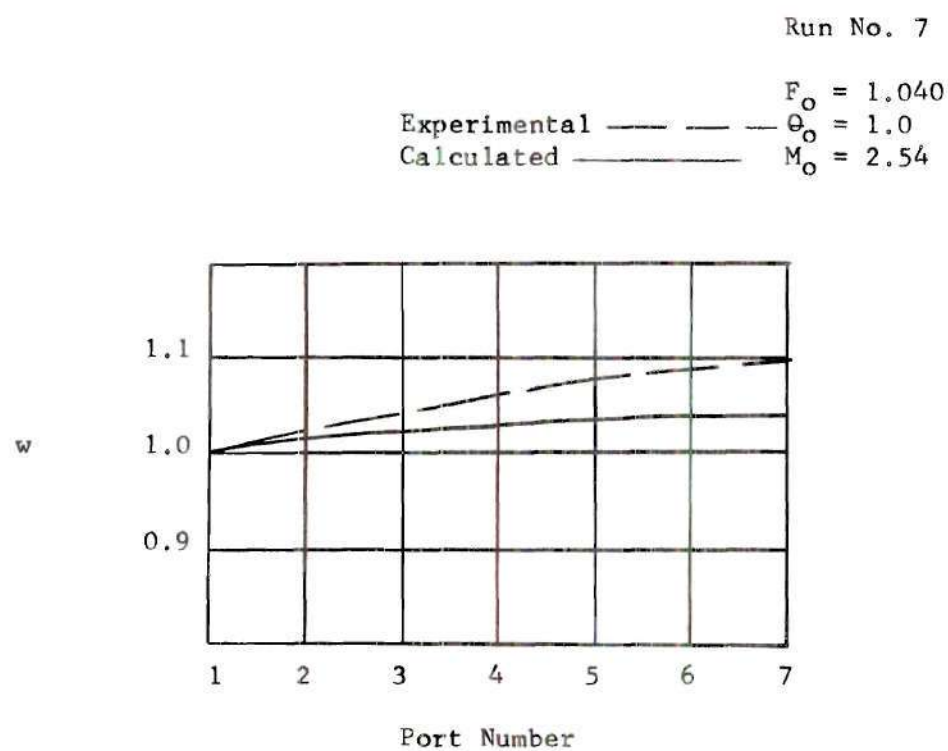


Figure 45. Comparison Between Experimental and Calculated Side Flow Distribution

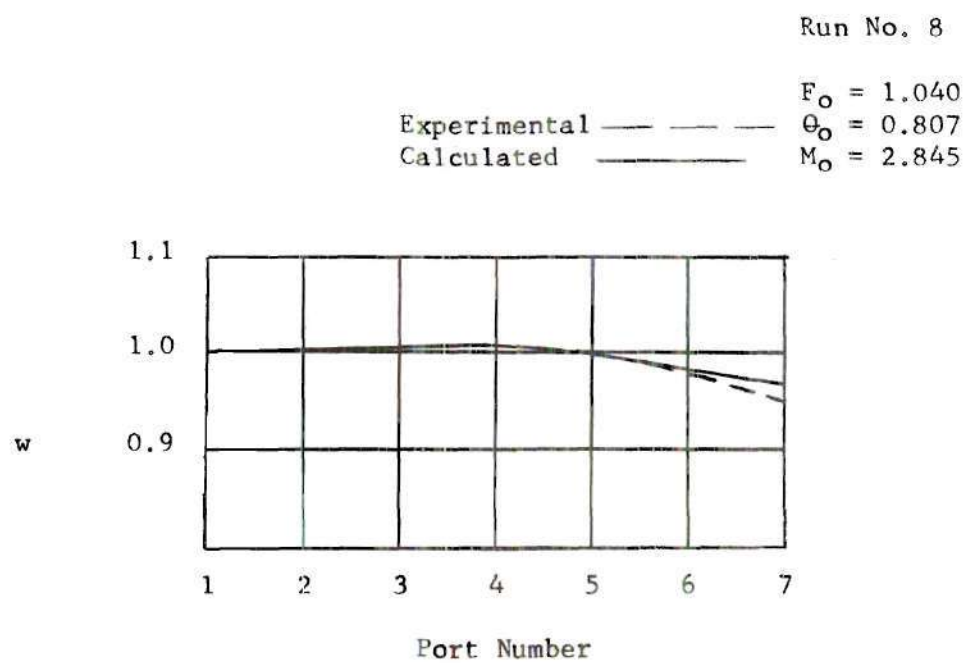


Figure 46. Comparison Between Experimental and Calculated Side Flow Distribution

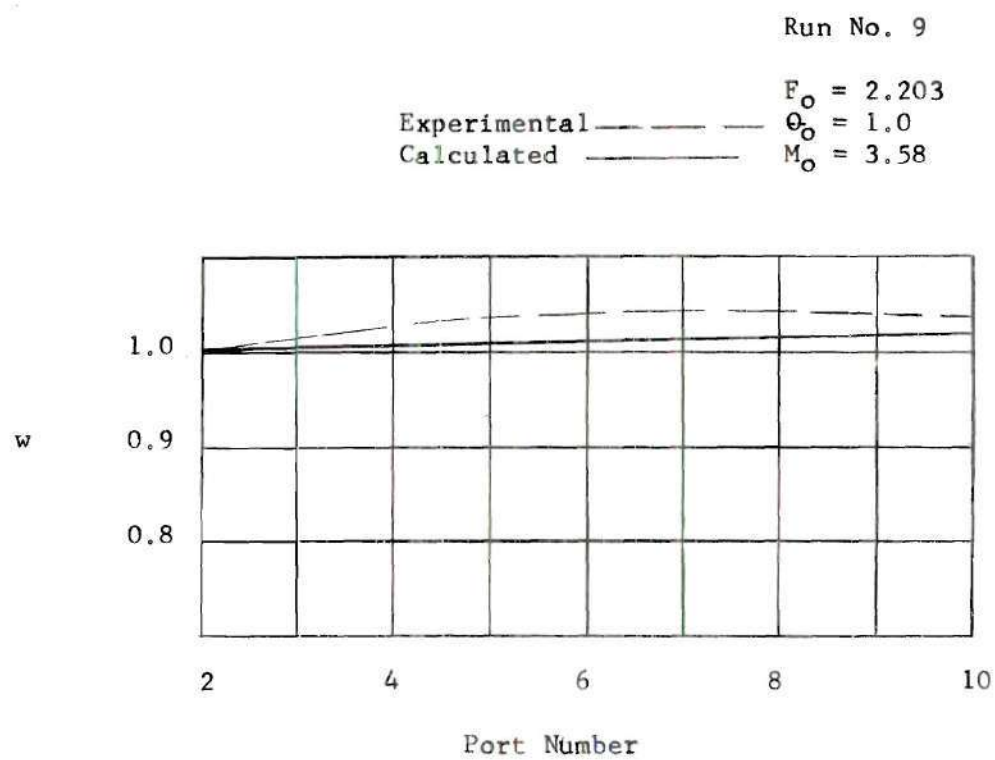


Figure 47. Comparison Between Experimental and Calculated Side Flow Distributions

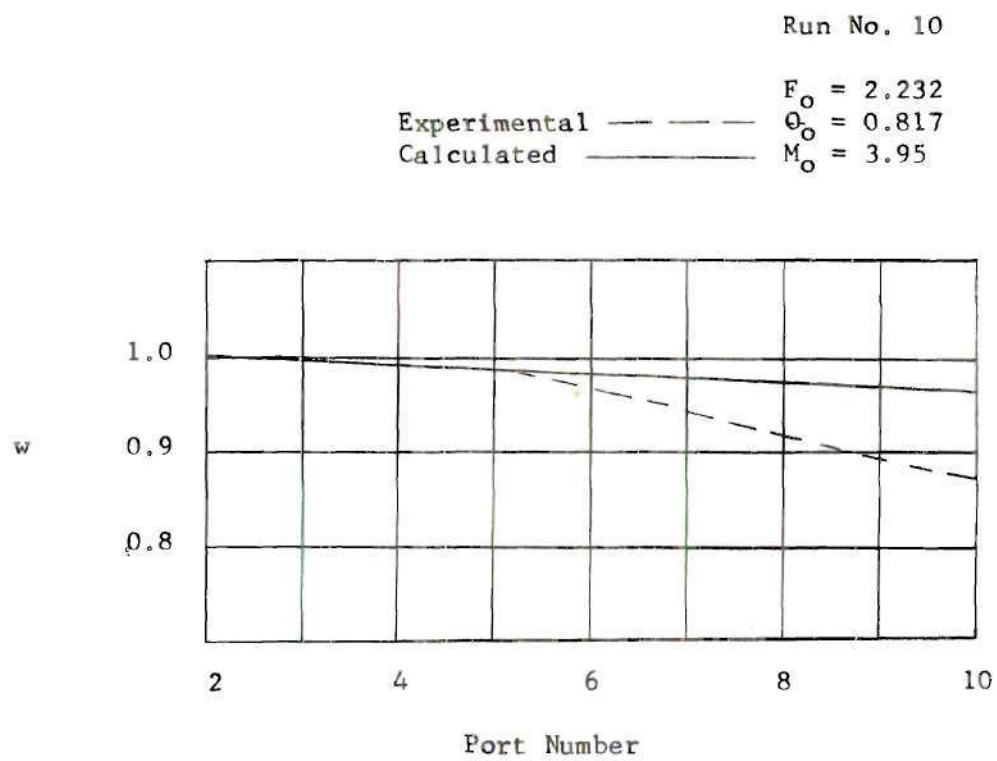


Figure 48. Comparison Between Experimental and Calculated Side Flow Distribution

## APPENDIX IV

## SAMPLE PROBLEM

Air, at  $100^{\circ}\text{F}$ , enters a manifold system at the rate of 25 cfm. The manifold is 70 inches long with 4 exhaust ports. The run is 1-1/4 inch, 14 BWG gage tubing, with an inside diameter of 1.084 inches, and the discharge is through 5/8-inch, 18 BWG gage tubing with an inside diameter of 0.527 inches. Determine the inlet pressure required and the variation in the flow distribution.

$$u_o = \frac{Q_o}{A} = \frac{4Q_o}{\pi D^2} = \frac{(4)(25) \frac{1}{60}}{(\pi)(1.084)^2 \frac{1}{144}}$$

$$u_o = \frac{(4)(25)(144)}{(\pi)(1.084)^2(60)} = \frac{14400}{221.5} = 65.01 \frac{\text{ft}}{\text{sec}}$$

For air near atmospheric pressure,  $\nu = 0.180 \times 10^{-3} \text{ ft}^2/\text{sec}$

$$\text{Re} = \frac{u_o D}{\nu} = \frac{(65.01)(1.084)}{(12)(0.180 \times 10^{-3})} = \frac{70.47}{0.00216}$$

$$\text{Re} = 32,600$$

for commercial pipe, relative roughness approximately 0.00015

$$f_o = 0.00582$$

$$F = f_o \quad \text{Now for } \beta = K = 0.6$$

$$\frac{2^{5/2} \beta^{3/2} \propto K}{}$$

$$F_o = \frac{0.00582}{(1.2)^{5/2} \propto} = \frac{(0.00582)}{(1.577) \propto}$$

$$F_o = \frac{0.00369}{\alpha}$$

$$\alpha = \frac{nd^2}{4DL} = \frac{(4)(0.527)^2}{(4)(1.084)(70)} = \frac{0.2777}{75.88}$$

$$\alpha = 0.00366$$

$$F = \frac{0.00369}{0.00366} = 1.008$$

$$L^* = 4\alpha K \sqrt{2\beta} \frac{L}{D} = (4)(0.00366)(0.6)(\sqrt{1.2}) \frac{(70)}{(1.084)}$$

$$L^* = 0.621$$

$$\theta_o = \frac{T_o}{T_w} = \frac{100+460}{240+460} = \frac{560}{700}$$

$$\theta_o = 0.8$$

from Figure 27  $M_o = 1.45$

from Figure 21 Max variation, 16%

$$p_o^o = \frac{M_o^2}{2}$$

$$\frac{p_o^o - p_s}{2\beta\rho_o u_o^2} = \frac{M_o^2}{2}$$

$p_o^o - p_s = p_{go}$  where  $p_{go}$  is the gage pressure at the inlet to the manifold

$$p_{go} = M_o^2 \beta \rho_o u_o^2$$

for air at atmospheric pressure and 100° F,  $\rho = 0.071 \text{ lbm/ft}^3$

$$\rho = \frac{0.071}{32.2} = 0.0022 \frac{\text{slugs}}{\text{ft}^3}$$

$$p_{go} = (1.45)^2 (0.6) (0.0022) (65.01)^2$$

$$p_{go} = 11.73 \frac{\text{lbf}}{\text{ft}^2}$$

$$p_{go} = 0.0815 \text{ psi}$$



## NOMENCLATURE

$A$	- Cross-sectional area of manifold
$D$	- Diameter of the manifold
$p_s$	- Uniform pressure outside the discharge port
$p_i^o$	- The pressure at the left end of the straight tube section $i$ *
$p_i^i$	- The pressure at the right end of the straight tube section $i$
$R$	- Gas constant
$T_i$	- Absolute temperature at port $i$
$T_o$	- Absolute temperature of the fluid entering the manifold
$T_w$	- Absolute temperature of the manifold wall
$T^o$	- Absolute stagnation temperature of the fluid
$u$	- The velocity in the straight tube section. The same convention applies to subscripts and superscripts as for the pressure.
$x$	- The distance from the beginning of the manifold $\Delta x$ is the distance between ports
$\mu$	- Absolute viscosity
$\rho$	- Density of fluid in slugs/ft <sup>3</sup>

Dimensionless Quantities

$\bar{a}$	- $1 - \theta_o$
$C$	- Coefficient for variation of viscosity with the absolute temperature

---

\*This notation is for the flow moving from left to right and port  $i$  preceding tube section  $i$ .

$f_i$  - Fanning friction factor

$$F_i = \frac{f_i}{2^{5/2} \beta^{3/2} \alpha_K}$$

$$G_i = \frac{1}{2\beta} \ln \left( \frac{\theta_{i+1}}{\theta_i} \right)$$

$k$  - Ratio of specific heats

$K$  - Coefficient of discharge for the orifice equation, applied to the side port

$L^0$  - Dimensionless length ( $4\alpha_K \sqrt{2\beta} \frac{L}{D}$ )

$M$  - Mach number

$$M_o^2 = \frac{p_o - p_s}{\beta \rho_o u_o^2}$$

$N$  - Exponent defining the relationship of  $F_i$  as a function of  $Re$

$$P_i^o = \frac{(p_i^o - p_s)}{2\beta \rho_o u_o^2}$$

$Re$  - Reynolds number

$$U_i^o = \frac{u_i^o}{u_o}$$

$w$  - Side flow rate/initial side flow rate

$$y = \left( \frac{4\alpha_K}{D} \sqrt{2\beta} \right) x$$

$\alpha$  - The fraction of the internal surface area of the tube that is occupied by discharge ports, assumed uniformly spaced along the tube  $\alpha \pi D \Delta x$  = discharge area of the port

$\beta$  - The coefficient of pressure recovery as applied to the discharge port

$$\theta_1 = \frac{T_1}{T_w}$$

$$\theta_1 = \frac{p_1}{p_o}$$

## BIBLIOGRAPHY

1. Keller, J. D.; Journal of Applied Mechanics, V. 16, N. 1, 77-85 March 1949.
2. Dow, W. M.; Journal of Applied Mechanics, V. 17, N. 4, 431-438 December 1950.
3. Acrivos, A., Babcock, B. D., Pigford, R. L.; Chemical Engineering Science, V. 10, 112-124, (1959).
4. Allen, J., Albinson, B.; Proceedings Institute of Civil Engineers (London), V. 4, Pt. 3, 114-138, (1955).
5. Safar, L. A.; Effect of Heating Upon Mass Flow Rate Through Ports of a Manifold, M.S. Thesis, Georgia Institute of Technology, 1957, p. 54.
6. Shapiro, A. H.; The Dynamics and Thermodynamics of Compressible Fluid Flow, Vol. 1, Ronald Press (1953). Chapter 8, pp. 219-260.

Other References:

7. American Gas Association, Combustion, Mack Printing Company, Easton, Pa., 3rd Edition, 1932, pp. 122, 132-134.
8. Batin, N. A.; "The Calculation of Branching Pipelines", (Russian) Sb. Nauch. Tr. Belorus. Lesotekhn. In-ta No. 8, (1956) p. 149-164.
9. Berman, A. S.; "Laminar Flow in an Annulus with Porous Walls", Journal of Applied Physics, Vol. 29, No. 1, p. 71-75, January 1958.
10. Ellms, J. W.; Journal of the American Water Works Association, Vol. 18, December 1927, p. 664.
11. Enger and Levy; Ibid, Vol. 21, No. 5, May 1929, p. 659.
12. Howland, W. E.; "Design of Perforated Pipe for Uniformity of Discharge", Proceedings Third Midwest Conference on Fluid Mechanics, (1953), p. 687.
13. Horlock, J. H.; "An Investigation of the Flow in Manifolds with Open and Closed Ends", Journal Royal Aeronautical Society, Vol. 60, (1956), p. 749.
14. Markland, E.; "The Analysis of Flow from Pipe Manifolds", Engineering, Vol. 187, No. 4847, January 1959, p. 150-1.

15. Moore, W. L.; "Relationships Between Pipe Resistance Formulas", Proceedings of the American Society of Civil Engineers, Vol. 85, Hy 3, p. 25-41, March 1959.
16. Noyes, R. N.; "An Exact Solution of the Compressible Flow Characteristics in Constant Area Passages with Simultaneous and Constant Heat Flux", Transactions of the American Society of Mechanical Engineers, Journal of Heat Transfer, Vol. 83, Series C, No. 4, Nov. 1961, p. 454.
17. Olson, F. C. W.; "Flow Through a Pipe with a Porous Wall", Transactions of the American Society of Mechanical Engineers, Vol. 71, 1949, pp. 53-54.
18. Weissberg, H. L.; "Laminar Flow in the Entrance Region of a Porous Pipe", The Physics of Fluids, Vol. 2, No. 5, September-October 1959.
19. Weissberg, H. L.; Velocity and Pressure Distributions in Turbulent Pipe Flow with Uniform Wall Suction, Report No. K-1187, Carbide and Carbon Chemical Company, Oak Ridge, Tennessee, March 29, 1955.
20. Weissberg, H. L.; Velocity Profiles and Friction Factors for Turbulent Pipe Flow with Uniform Wall Suction, Report No. K-1264, Carbide and Carbon Chemical Company, Oak Ridge, Tennessee, April 1956.
21. White, F. M., Jr.; Laminar Flow in Porous Ducts, Ph.D. Thesis, Georgia Institute of Technology, 1959, P. 75.
22. Wills, F.; "Design of Gas Burners by the Use of Fundamental Flow Formulae", Western Gas, Vol. 7, 1931, pp. 87-89.
23. Yuan, S. W.; "Turbulent Flow in Circular Pipe with Porous Wall", Physics of Fluids, Vol. 4, No. 3, March 1961, p. 368-72.



## VITA

Roy Warner Blanton, Jr., son of Jane Boland Blanton and Roy Warner Blanton, was born on May 29, 1935, in Columbus, Georgia. In 1946 he moved with his family to Albany, Georgia, where he completed elementary school and attended high school.

Upon graduation from Albany High School in 1953, he enrolled at Emory University, Atlanta, Georgia. In 1955, he transferred to the Georgia Institute of Technology, Atlanta, Georgia, where he enrolled in the School of Mechanical Engineering. He received the Bachelor of Mechanical Engineering Degree in 1958.

Upon completion of the undergraduate curriculum in 1957, he enrolled in graduate school at the Georgia Institute of Technology in the School of Mechanical Engineering. He received the Master of Science in Mechanical Engineering in 1959. The title of his Master of Science thesis is "Radiant Energy Exchange Configuration Factors for Non-Lambertian Surfaces."

He continued with his graduate work upon completion of the Master of Science degree, and joined the Staff of the School of Mechanical Engineering from 1958 until 1961. During this period he instructed undergraduate courses in Fluid Mechanics, Heat Transfer, and Thermodynamics.

He is married to the former Miss Estelle Maloy of Atlanta, Georgia, and is the father of one son, Steven Edward Blanton.

He is a member of the following honorary fraternities:

Pi Tau Sigma

Tau Beta Pi

Phi Kappa Phi

The Society of Sigma Xi

Upon completion of the residency requirements for the degree of Doctor of Philosophy in Mechanical Engineering in 1962, he joined Roy W. Blanton Sales & Engineering, Albany, Georgia, as Vice-President.